

UC Berkeley

UC Berkeley Previously Published Works

Title

CRYSTAL GROWTH. Crystallization by particle attachment in synthetic, biogenic, and geologic environments.

Permalink

<https://escholarship.org/uc/item/1n55m9r9>

Journal

Science (New York, N.Y.), 349(6247)

ISSN

0036-8075

Authors

De Yoreo, James J
Gilbert, Pupa UPA
Sommerdijk, Nico AJM
[et al.](#)

Publication Date

2015-07-01

DOI

10.1126/science.aaa6760

Peer reviewed

Crystallization by particle attachment in synthetic, biogenic, and geologic environments

1. James J. De Yoreo^{1,2},
2. Pupa U. P. A. Gilbert^{3,4,*},
3. Nico A. J. M. Sommerdijk^{3,6},
4. R. Lee Penn⁷,
5. Stephen Whitelam⁸,
6. Derk Joester⁹,
7. Hengzhong Zhang¹⁰,
8. Jeffrey D. Rimer¹¹,
9. Alexandra Navrotsky¹²,
10. Jillian F. Banfield¹⁰,
11. Adam F. Wallace¹³,
12. F. Marc Michel¹⁴,
13. Fiona C. Meldrum¹⁵,
14. Helmut Cölfen¹⁶,
15. Patricia M. Dove^{†,14}

See all authors and affiliations

DOI: [10.1126/science.aaa6760](https://doi.org/10.1126/science.aaa6760)

- [Article](#)
- [Figures & Data](#)
- [Info & Metrics](#)
- [eLetters](#)
- [PDF](#)

Growing crystals by attaching particles

Crystals grow in a number of ways, including pathways involving the assembly of other particles and multi-ion complexes. De Yoreo *et al.* review the mounting evidence for these nonclassical pathways from new observational and computational techniques, and the thermodynamic basis for these growth mechanisms. Developing predictive models for these crystal growth and nucleation pathways will improve materials synthesis strategies. These approaches will also improve fundamental understanding of natural processes such as biomineralization and trace element cycling in aquatic ecosystems.

Science, this issue [10.1126/science.aaa6760](https://doi.org/10.1126/science.aaa6760)

Structured Abstract

BACKGROUND

Numerous lines of evidence challenge the traditional interpretations of how crystals nucleate and grow in synthetic and natural systems. In contrast to the monomer-by-monomer addition described in classical models, crystallization by addition of particles, ranging from multi-ion complexes to fully formed nanocrystals, is now recognized as a common phenomenon. This diverse set of pathways results from the complexity of both the free-energy landscapes and the reaction dynamics that govern particle formation and interaction.

Whereas experimental observations clearly demonstrate crystallization by particle attachment (CPA), many fundamental aspects remain unknown—particularly the interplay of solution structure, interfacial forces, and particle motion. Thus, a predictive description that connects molecular details to ensemble behavior is lacking. As that description develops, long-standing interpretations of crystal formation patterns in synthetic systems and natural environments must be revisited.

Here, we describe the current understanding of CPA, examine some of the nonclassical thermodynamic and dynamic mechanisms known to give rise to experimentally observed pathways, and highlight the challenges to our understanding of these mechanisms. We also explore the factors determining when particle-attachment pathways dominate growth and discuss their implications for interpreting natural crystallization and controlling nanomaterials synthesis.

ADVANCES

CPA has been observed or inferred in a wide range of synthetic systems—including oxide, metallic, and semiconductor nanoparticles; and zeolites, organic systems, macromolecules, and common biomineral phases formed biomimetically. CPA in natural environments also occurs in geologic and biological minerals. The species identified as being responsible for growth vary widely and include multi-ion complexes, oligomeric clusters, crystalline or amorphous nanoparticles, and monomer-rich liquid droplets.

Particle-based pathways exceed the scope of classical theories, which assume that a new phase appears via monomer-by-monomer addition to an isolated cluster. Theoretical studies have attempted to identify the forces that drive CPA, as well as the thermodynamic basis for appearance of the constituent particles. However, neither a qualitative consensus nor a comprehensive theory has emerged. Nonetheless, concepts from phase transition theory and colloidal physics provide many of the basic features needed for a qualitative framework. There is a free-energy landscape across which assembly takes place and that determines the thermodynamic preference for particle structure, shape, and size distribution. Dynamic processes, including particle diffusion and relaxation, determine whether the

growth process follows this preference or another, kinetically controlled pathway.

OUTLOOK

Although observations of CPA in synthetic systems are reported for diverse mineral compositions, efforts to establish the scope of CPA in natural environments have only recently begun. Particle-based mineral formation may have particular importance for biogeochemical cycling of nutrients and metals in aquatic systems, as well as for environmental remediation. CPA is poised to provide a better understanding of biomineral formation with a physical basis for the origins of some compositions, isotopic signatures, and morphologies. It may also explain enigmatic textures and patterns found in carbonate mineral deposits that record Earth's transition from an inorganic to a biological world.

A predictive understanding of CPA, which is believed to dominate solution-based growth of important semiconductor, oxide, and metallic nanomaterials, promises advances in nanomaterials design and synthesis for diverse applications. With a mechanism-based understanding, CPA processes can be exploited to produce hierarchical structures that retain the size-dependent attributes of their nanoscale building blocks and create materials with enhanced or novel physical and chemical properties.

- [Download high-res image](#)
- [Open in new tab](#)
- [Download Powerpoint](#)

Major gaps in our understanding of CPA.

Particle attachment is influenced by the structure of solvent and ions at solid-solution interfaces and in confined regions of solution between solid surfaces. The details of solution and solid structure create the forces that drive particle motion. However, as the particles move, the local structure and corresponding forces change, taking the particles from a regime of long-range to short-range interactions and eventually leading to particle-attachment events.

Abstract

Field and laboratory observations show that crystals commonly form by the addition and attachment of particles that range from multi-ion complexes to fully formed nanoparticles. The particles involved in these nonclassical pathways to crystallization are diverse, in contrast to classical models that consider only the addition of monomeric chemical species. We review progress toward understanding crystal growth by particle-attachment processes and show that multiple pathways result from the interplay of free-

energy landscapes and reaction dynamics. Much remains unknown about the fundamental aspects, particularly the relationships between solution structure, interfacial forces, and particle motion. Developing a predictive description that connects molecular details to ensemble behavior will require revisiting long-standing interpretations of crystal formation in synthetic systems, biominerals, and patterns of mineralization in natural environments.

The central roles of crystallization in geochemical, biological, and synthetic materials systems have motivated decades of research into crystal nucleation and growth. Since the mid-1900s, most studies have interpreted the results through the lens of classical nucleation theory ([1](#)) and the terrace-ledge-kink model of crystal growth ([2](#)), both of which are based on monomer-by-monomer addition of simple chemical species. Despite the successes of classical nucleation and growth models ([3](#), [4](#)), there are a number of phenomena associated with crystal formation that cannot satisfactorily be explained or predicted either quantitatively or qualitatively. For example, amorphous phases are reported to nucleate at concentrations well below those predicted by classical models ([5](#)). Equally perplexing are the irregular and branched crystal morphologies observed in synthetic nanocrystals ([6](#)) and the habits and microstructures of biominerals found in organisms ([7](#)). Similarly, the geologic record shows extensive mineral deposits with unusual mineralogical and textural patterns ([8](#)) that are not readily interpreted within the framework of classical mineral formation processes.

These characteristics have been attributed to nonclassical ([9](#)) crystal growth processes that are distinct from those envisioned by the traditional models. For example, mineralization of sea urchin embryonic spicules proceeds by accumulation of nanoparticles of an amorphous calcium carbonate (ACC) precursor, which subsequently transforms into a crystal of calcite ([10](#), [11](#)). Similar amorphous-to-crystalline pathways occur in diverse biominerals, including sea urchin spines ([12](#)) and teeth ([13](#)), mammalian tooth enamel ([14](#)), vertebrate bones ([15](#)), crustacean exoskeletons ([16](#)), annelid calcareous concretions ([17](#)), and mollusk larval shells ([18](#)). Likewise, aggregation of poorly ordered precursors precedes formation of biogenic magnetite ([19](#)) and zeolites ([20](#)), and biomimetic polymers introduced as proxies for biological macromolecules induce formation of liquid phases that transform into crystalline products through aggregation and dehydration ([21](#)).

Another nonclassical mechanism of crystal growth, oriented attachment (OA), proceeds by repeated attachment events of crystalline particles on specific crystal faces that are lattice-matched, either with true crystallographic alignment or across a twin boundary or stacking fault ([22](#)). Similarly, mesocrystals, which are kinetically stabilized superstructures of

nanocrystals in crystallographic alignment ([23](#), [24](#)), form as intermediates between dispersed particles and true single crystals. They may fuse and transform into single crystals ([24](#)) or remain kinetically stabilized by adsorbates—often polymeric—at the particle interfaces ([9](#)). Structured macromolecules can promote the OA process. For example, mineral precursors of tooth enamel assemble in vitro into chains with co-orientation imparted by structured protein oligomers within which the mineral resides before fusion into single-crystal rods ([25](#)).

These discoveries show that in many systems, crystallization can occur by attachment of a wide range of species more complex than simple ions ([Fig. 1](#)). We refer to these higher-order species as particles, broadly defined to include multi-ion complexes ([5](#)), oligomers (or clusters) ([26](#)), and nanoparticles—whether crystalline ([27](#)), amorphous ([14](#)), or liquid ([21](#)). We review the current understanding of crystallization by particle attachment (CPA) and examine thermodynamic and dynamic mechanisms that give rise to CPA. Our analysis also explores the intrinsic and extrinsic factors that determine when particle-based pathways dominate growth. Although many of the principles discussed here are likely to apply to organic and macromolecular crystals, such as the involvement of liquid precursors, this examination of CPA is largely restricted to inorganic systems, both because the study of inorganic crystal growth by CPA is more mature at this time and because the conformational degrees of freedom in macromolecular systems introduce dynamical factors that render them distinct from inorganic systems. Looking ahead, we identify areas where our mechanistic understanding is weak and highlight directions for future research.

- [Download high-res image](#)
- [Open in new tab](#)
- [Download Powerpoint](#)

Fig. 1 Pathways to crystallization by particle attachment.

In contrast to monomer-by-monomer addition as envisioned in classical models of crystal growth (gray curve), CPA occurs by the addition of higher-order species ranging from multi-ion complexes to fully formed nanocrystals. (The final faceted bulk crystal is a schematic representation of a final single-crystal state. As [Figs. 2](#) and [3](#) show, the final crystal can have more complex morphologies, including spheroidal.)

Evidence, indicators, and consequences of crystallization by particle attachment

In situ observations of crystal growth from solution at a resolution where the atomic-scale lattice and the addition of growth units are observable are rare and generally limited to liquid-phase scanning probe (28) and transmission electron microscope (TEM) (27, 29, 30) studies. Consequently, there are very few systems in which CPA has been unequivocally demonstrated, and most evidence is based on observations of crystals made after the pathway from solvated state to crystal phase has been traversed. Nonetheless, static images showing apparent assemblies of coaligned nanocrystals (Fig. 2A) have been frequently accepted as evidence for CPA via OA. Moreover, definitive confirmation of OA through in situ liquid-phase electron microscopy (Fig. 2, B and C) in both oxide and metallic systems (27, 29) forms a basis for inferring its occurrence from features observed ex situ.

- [Download high-res image](#)
- [Open in new tab](#)
- [Download Powerpoint](#)

Fig. 2 Examples of inorganic crystals formed by CPA.

(A) Nanoparticles of anatase (TiO_2) with perfect alignment after apparent attachment event with the c axis oriented along the long dimension of the aggregate (116). (B and C) Sequential in situ images showing oriented attachment of ferrihydrite with creation of an edge dislocation (yellow lines) and resulting tilt of lattice planes above and below the edge dislocation (red lines) (27, 30). (D to F) TiO_2 nanocrystals showing defects incorporated through CPA, including (D) low-angle tilt boundaries, (E) screw dislocations, and (F) twin planes. In (E), the variations in contrast and slight shift in lattice fringe clarity and alignment indicate incorporation of defects. The blue lines highlight the orientation and shift in lattice fringe alignment to either side of the region that contains the dislocations; the bright-dark contrast is consistent with a dislocation having a screw component. (G) Branched nanowire of rutile (TiO_2), where each branch occurs on a set of twin boundaries (inset) (60). (H) Single-crystal honeycomb superlattice formed through oriented attachment of PbSe nanocrystals in an octahedral symmetry. The equilateral triangle shows the long-range ordering of the structure, and the inset shows the relationship of the crystalline axes with the superlattice pattern (39) (I) Cryo-TEM micrograph of a single zeolite nanoparticle (117). (J) Atomic force micrograph of a zeolite surface showing that its growth proceeds by attachment of silica nanoparticles (28). (K) Calcium phosphate prenucleation complexes aggregating to form amorphous calcium phosphate nanoparticles. (Inset) Amorphous calcium phosphate nanoparticle is replaced by outgrowths of calcium-deficient octacalcium phosphate (5). (L) Magnetite crystal growing through the accretion of disordered ferrihydrite-like nanoparticles (57). (M) Goethite mesocrystal

formed by the assembly of nanocrystals shows lattice fringes that correspond to (021) planes ([62](#)).

Electron microscopy—particularly cryogenic TEM (cryo-TEM)—of synthetic crystals has proven to be highly valuable for characterizing features associated with CPA ([Fig. 2](#)). TEM images have revealed primary particles ranging from crystalline ([Fig. 2, A to F](#)) to partially ordered ([Fig. 2, I and L](#)) to wholly amorphous ([Fig. 2K](#)). These images have provided indicators of CPA in both secondary particles and fully formed crystals, including chainlike ([Fig. 2A](#)) and branched ([Fig. 2G](#)) morphologies that defy expectations based on crystal symmetry ([Fig. 2, A, F, G, I, and M](#)). Other indicators provided by TEM are rounded protrusions comparable in size to the primary particles residing in the crystallizing solution ([Fig. 2, B, C, and I to L](#)), internal pores ([Fig. 2H](#)), the retention of apparent interfaces between primary particles ([Fig. 2, D to G](#)), and incorporation of defects at these inferred interfaces. Defects can consist of dislocations ([Fig. 2D](#)) that form due to small misalignments during attachment ([Fig. 2B](#)) and twin planes or stacking faults that reflect attachment of particles along symmetry-related lattice vectors ([Fig. 2F](#)). Defects can also be eliminated through the rearrangement or recrystallization of primary particles after their aggregation ([Fig. 2, C, I, J, and L](#)).

The potential role of CPA in biomineral formation has been widely discussed and is often conjectured based on external morphologies and/or internal microstructure. In certain cases, evidence comes from both nanoscale imaging and spectroscopic documentation of phases ([10–12, 14, 15](#)) ([Fig. 3](#)). As in the case of synthetic crystals, the resulting structures exhibit unexpected morphologies ([Fig. 3, A to D](#)) and internal microstructure ([Fig. 3, A to D](#)). In all of these cases, the primary particles are amorphous ([Fig. 3, A, B, and E](#)).

- [Download high-res image](#)
- [Open in new tab](#)
- [Download Powerpoint](#)

Fig. 3 Examples of biogenic crystals proposed to form by aggregation of nanosized particles.

(A) Photoelectron emission microscopy component map of the mineral phases in sea urchin embryonic spicules: ACC-H₂O (red), ACC (green), and calcite (blue) ([11](#)). (B) Component maps of sea urchin spicules at three different developmental stages: At 36 hours, the dominant phase is ACC-H₂O; at 48 hours, it is ACC; and at 72 hours, it is calcite. (C) Cryo-fractured surface of a sea urchin spicule from *Strongylocentrotus purpuratus*. The inset shows

a lower magnification micrograph of the same portion of a spicule. **(D)** Field-emission scanning electron microscope (FE-SEM) micrograph of terraced nacre tablets from the mollusk shell of *Pinctada fucata*, which are made of aragonite nanoscale building blocks ([118](#)). **(E and F)** Cryo-SEM micrographs of the bone growth zone in high-pressure frozen fin tissue of the zebrafish (*Danio rerio*). Newly deposited, nonmineralized bone matrix contains large, mineral-bearing globules, which fuse into the mineralizing bone matrix (black arrow) ([119](#)). These globules fuse into the mineralizing bone. Spectroscopic measurements show that the edges of the forming bone are amorphous calcium phosphate, whereas the bone region is crystalline hydroxyapatite. **(F)** Higher magnification of area delineated by the box in **(E)**, showing post-attachment particulate substructure of a globule.

Although external morphology (e.g., [\(Fig. 2, I and J\)](#), and [\(Fig. 3D\)](#), microstructure, and texture provide important evidence of attachment-based growth, they alone do not prove formation by a particle-based growth process. In fact, such features can be misleading. For example, irregular or branched morphologies can form through dendritic and spherulitic growth mechanisms from solution at high supersaturation ([31](#)). Such solids can retain pores, branches, and rounded features formed during growth. Moreover, crystals grown through classical mechanisms within physical templates ([32](#)) or with the addition of organic polymers ([33](#)) can exhibit similar morphologies to those seen in natural biominerals and in synthetic crystals attributed to CPA, so interpreting particulate-like morphologies in terms of pathways requires other substantiating evidence. Conversely, even when formation pathways are dominated by particle addition in the early stages, coarsening or recrystallization can subsequently obliterate characteristic signatures ([34](#)). Thus, the absence of such features is not conclusive evidence of monomer-by-monomer growth. As a result, a holistic suite of characterization techniques is essential to building a strong case for CPA in any given system. Combinations of direct imaging, scattering, and spectroscopy—particularly data collected at different time points throughout crystallization that can detail the kinetics of growth—imply that CPA is a prevalent growth mechanism at the early stages of crystallization ([5](#), [11](#), [35–37](#)).

Particle-based pathways have important consequences for the structure and properties of materials. They can lead to unique morphologies ([Fig. 2, A and G to I](#), and [Fig. 3, A, C, and D](#)), nonequilibrium symmetries ([Fig. 2, F to H](#), and [Fig. 3, D and E](#)), distinct internal defect distributions ([Fig. 2, C to F](#), and [Fig. 3, A, B, and D](#)), and organic-inorganic hybrid structures in which the coaligned nanoparticles are surrounded by organic matter ([9](#), [38](#), [39](#)) ([Fig. 2H](#) and [Fig. 3, E and F](#)). In addition, crystals formed by CPA can presumably exhibit heterogeneous distributions of elements composing the crystals, either because the primary particles have distinct compositions or because species that formerly resided on primary

nanoparticle surfaces are incorporated at the interface generated during attachment events. The stability, mechanical behavior, surface adsorption, transport, catalytic activity, and optical properties of nanomaterials should all depend critically on such characteristics.

Interplay of thermodynamics and kinetics lead to key features of CPA

Despite the structural diversity of the particles involved in CPA, key features of many crystallization pathways can be understood by considering the interplay of free-energy landscapes and reaction dynamics ([Fig. 4](#)). The first of these determines the thermodynamic preference for the structure, shape, and size distribution of particles at various stages of assembly. Dynamic processes, in turn, including monomer and particle diffusion and internal particle relaxation, determine whether this set of preferences occurs or whether an alternate, kinetically controlled pathway is traversed.

- [Download high-res image](#)
- [Open in new tab](#)
- [Download Powerpoint](#)

Fig. 4 Crystallization by a wide variety of pathways.

The possible pathways by which monomers form a stable bulk crystal, and the physical mechanisms that give rise to them, can have thermodynamic (**A** to **C**) and kinetic (**D** and **E**) origins. Each of the pathways in [Fig. 1](#) can be associated with the mechanisms shown here. (A) Classical monomer-by-monomer addition. (B) Aggregation of metastable particles, such as liquid, amorphous, or poorly crystalline particles, or of oriented (and nearly oriented) attachment of metastable nanocrystals. (C) Crystallization via the formation of a metastable bulk phase, such as a liquid or solid polymorph. (D) Kinetically dominated aggregation of clusters or oligomers. (E) Aggregation of unstable particles whose internal structures are not those of equilibrium phases. The phase diagrams (**F**), with or without a spinodal region, reflect thermodynamic controls on assembly. As indicated, each pathway in (A) through (E) corresponds to a similarly labeled point in these phase diagrams. Modified after ([51](#)).

Monomers dispersed in solution that interact through Brownian motion can aggregate to form larger structures via a wide variety of pathways ([Fig. 4, A to E](#)), which can be correlated with distinct points in typical phase diagrams (identified by the labels A to E in [Fig. 4F](#)). These pathways may be simple, comprising monomer-by-monomer addition to incipient nuclei that display a

single structure (**Fig. 4A**). However, they may also be complex, involving particles (**Fig. 4, B and C**) that may be structurally distinct from the final, thermodynamically stable, bulk phase (e.g., **Fig. 2, G, K, and L**, and **Fig. 3, A and B**).

The magnitude of the free-energy barrier to nucleation with respect to the thermal energy, $k_B T$, is a crucial factor in determining the number and nature of particles produced. As the free-energy barrier varies in shape and magnitude, there is a change from monomer-based (**Fig. 4A**) to particle-based (**Fig. 4, B to E**) pathways (**40**). At low supersaturation (**Fig. 4A**), the free-energy barrier is relatively large. The generation of a critical nucleus is then a rare event, and any particles that nucleate are unlikely to see other particles in their immediate vicinity. Thus, one observes a monomer-by-monomer nucleation-and-growth pathway assumed by classical nucleation theories (**1**).

As supersaturation increases (**Fig. 4D**), the free-energy barrier to phase change diminishes and particles are generated in greater numbers. They can then grow (or shrink) by exchanging monomers with other particles, as well as through collision and occasional collision and coalescence events (**41**). When supersaturation is increased until the free-energy barrier is comparable with $k_B T$, the solution undergoes spinodal decomposition (**42, 43**), at which point the particles are generated in such large numbers that growth by direct collision and coalescence with other particles can dominate (**Fig. 4D**).

In the cases described above (**Fig. 4, A and D**), the free-energy landscape displays a barrier (large in the nucleation regime and small or nonexistent in the spinodal regime) but does not exhibit any features that would suggest the existence of multiple particles during nucleation. Thermodynamically speaking, the system should prefer to grow as one large particle. This is because particles have no special thermodynamic status: They are neither stable nor metastable; that is, they do not reside in a global or a local free-energy minimum. Nonetheless, multiple particles (**Fig. 4D**) appear for dynamic reasons, and this gives rise to particle-based pathways

If the free-energy landscape exhibits local minima (**Fig. 4B**), the formation of particles of particular sizes or morphologies becomes thermodynamically favored, and one can observe assembly pathways involving thermodynamically metastable particles that need not appear on a bulk phase diagram. Examples of such intermediates include the metastable aggregates of particles that form by the association of calcium phosphate complexes at high supersaturations, before their transformation to amorphous calcium phosphate (**5, 44**), and possibly the polymeric states predicted for calcium carbonate solutions (**26**).

Another type of complex assembly pathway involves thermodynamically metastable bulk phases that are subsequently replaced by more stable phases (45) (Fig. 4C). There are at least two distinct examples of this type of pathway. In the first, a metastable solid phase forms because the barrier to its nucleation is smaller than that opposing nucleation of the stable phase. Nucleation of the stable phase eventually occurs either heterogeneously on (or in) the metastable particles or homogeneously in the surrounding solution, leading to dissolution or recrystallization of the metastable phase, as is often observed, for example, in the calcium carbonate system (30, 46–48). This pathway is commonly referred to as the Ostwald-Lussac rule of stages or the Ostwald step rule. In the second example, monomers associate in an unstructured way, resulting in the formation of amorphous particles or, in the case of spinodal decomposition, of monomer-rich liquid droplets that subsequently crystallize. Such two-step pathways are seen during crystallization of proteins (49), of some inorganic electrolytes such as MgSO_4 (50), and in simple computer models of spheres with isotropic attractions (51). Two-step pathways via liquid precursors are also proposed for the CaCO_3 system based on electron microscopy (52), calorimetry and nuclear magnetic resonance (NMR) studies (53), and molecular dynamics simulations (40).

When the internal relaxation of metastable species is sufficiently slow, the formation of long-lived metastable or nonequilibrium materials such as gels becomes possible for dynamic reasons (Fig. 4E) either before or instead of the formation of a stable crystal (54). Moreover, hierarchical pathways that result in growth by OA reflect dynamic factors that bias attachment on specific faces, despite the fact that the global minimum in free energy is independent of such factors.

Thus, well-known physical mechanisms lead generically to a range of hierarchical and multistep assembly pathways, including monomer-by-monomer addition, often occurring simultaneously (27, 30). Nonetheless, interpretations of recent experimental observations and simulations raise new challenges to the classifications described above. For example, proposed pathways involving aggregation of stable “prenucleation cluster” species (26, 55) are inconsistent with the existing understanding of phase change that considers subcritical clusters to be unstable (Fig. 4A) or, perhaps, metastable (Fig. 4B).

The influence of surface energy on pathways

When the free-energy landscape includes multiple minima representing different polymorphs of the same crystal (Fig. 4D), the interfacial free energy (or surface energy) can have a large influence on pathways of CPA, because it affects the size of the free-energy barrier. (Here, we use the term polymorph to include hydrated phases of an otherwise identical

composition.) If the surface energy of the metastable polymorph is much smaller than that of the stable phase, then Ostwald's step rule is likely to be observed. However, if the differences in thermodynamic stability, and hence surface free energy, of two polymorphs are subtle or the supersaturations with respect to both polymorphs are high, then the free-energy barriers to nucleation of either can be so small that both will form. Particle-particle interaction and aggregation events can then involve particles of distinct phases ([56](#), [57](#)) (e.g., [Fig. 2, G and L](#), and [Fig. 3, A, B, and E](#)).

Although the relative stability of the polymorphs depends on bulk properties such as the enthalpy of formation and molar volume, the contribution of surface free energy often results in a dependence of stability on crystal size ([58](#), [59](#)). This dependence can even invert the sequence of polymorph stability relative to that observed for the bulk phases ([58](#)). Thus, primary particles may be a polymorph that is only stable at a small size, while the secondary particles have the structure of the stable bulk form ([34](#), [56](#), [57](#), [60](#)). That is, the free-energy barrier to nucleating small particles possessing a form that is metastable in the bulk phase will be lower than the barrier to nucleating particles of the same size possessing the stable bulk form. For CPA to generate single crystals in such systems, the attachment events must accommodate the structural differences between the two phases, either through a structural match at the interface ([60](#)) or through postattachment phase transformation ([34](#), [56](#), [57](#)).

Recent computational work suggests that the solvent plays important roles in mediating particle interactions and attachment events ([61](#)). Cryo-TEM observations showing coaligned arrays of particles that appear separated by a solvent layer underline the importance of the solvent in mediating attachment ([62](#)). Because the solvation energy of a surface generally becomes more exothermic with increasing surface energy ([59](#)), the dynamics of CPA should also be affected by surface energies. In particular, high-energy surfaces with loosely held solvent may be more reactive toward other species in the solution, including other particles. Meanwhile, surfaces to which solvation layers are strongly bound may resist attachment, thus biasing OA to occur on specific faces through the influence of kinetic barriers rather than attractive forces ([35](#), [61](#)). Understanding the role of surface energies in phase selection and structural transformation dynamics and relating surface and solvation energies to nucleation, reactivity, and assembly are major challenges still to be addressed.

Precursor phases

The inherent size dependence of thermodynamic drivers ([59](#), [63](#)) and the kinetic constraints placed on nucleation of polymorphs by the barriers in the energy landscape render precursor phases a ubiquitous feature of crystallizing systems ([58](#), [59](#)). Consequently, pathways to a final stable

phase via CPA often involve precursor particles (**Figs. 1** and **4**). Precursors can include one or more solid amorphous phases (**10, 12, 14, 15, 18, 30, 46, 64, 65**), dense liquids or gels (**21, 49, 53**), or crystalline nanoparticles (**30, 57, 60, 63**). Each results in a distinct growth history, but whether or not the final outcomes are also distinct should depend on the extent to which monomer-by-monomer addition competes with the particle-attachment pathways and coarsening or recrystallization processes modify the structure and morphology of the growing crystal.

Amorphous phases

Mineral systems may crystallize through an amorphous precursor at sufficiently high supersaturation (**5, 20, 46, 66–69**), but the mechanism of the transition is unclear for most systems. For calcium carbonate formed abiotically from aqueous solution, the ACC precursor phase is initially hydrated (**64, 66**). In the bulk, hydrated ACC is stable in dry conditions but crystallizes in humid conditions or upon heating with the release of water (**46, 70**). Although the observed coexistence of crystalline and amorphous material within early stage nanoparticles both in solution (**69**) and under Langmuir monolayers (**47**) suggests that solid-state crystallization may occur at the onset of the transition, ACC confined in small volumes remains stable for very long times even in the presence of bulk water, indicating that a heterogeneous nucleator for one of the crystalline polymorphs may be required (**71, 72**). Transformation then typically occurs through local dissolution and reprecipitation (**73**). Because the crystalline polymorphs have a much lower solubility than ACC, in environments free of bulk water, the release of water upon initiation of crystallization of the hydrated phase might then induce local dissolution and reprecipitation. Thus, water release and crystallization may be connected and could result in the appearance of microfacets during crystallization (**36, 48**). However, ACC can also dehydrate before the onset of crystallization (**64**), in which case faceting may not occur. The generality of this behavior is unclear because the extent to which amorphous phases of other materials contain solvent as a structural element is unknown. Moreover, when crystallite size becomes sufficiently small, the possibility that some materials may exist in a continuum across structural states from crystalline to amorphous has been suggested (**74**).

In biomineralization, crystallization from transient amorphous precursor particles is believed to be a widespread strategy that enables the efficient transport of mineral constituents with low solubility to the crystallization site (**75**). In cases involving ACC, research indicates that the nanoparticles—which in their initial, hydrated ACC form may be liquid- or gel-like but later dehydrate—likely serve as the initial precursor phase and become a space-filling material (**76**). The full mechanism of the transformation to crystal remains a subject of investigation (**11, 36, 77**).

Dense liquid droplets

Protein and polymer solutions often exhibit partial miscibility, with a dense liquid phase ([49](#), [78](#)) that can act as a precursor to crystal formation. The emergence of such a state, however, does not necessarily imply its active participation in crystallization. Aqueous electrolyte solutions may also undergo liquid-liquid phase separation at elevated temperatures ([50](#), [79](#)). In addition, a combination of calorimetry, nanoparticle tracking, NMR experiments ([53](#)) and in situ liquid phase TEM ([30](#)), and theoretical investigations ([40](#)) have provided evidence that a liquid-liquid phase separation occurs near room temperature in the CaCO_3 system. Liquid droplets produced by this mechanism should undergo aggregation events due to diffusion and collision ([40](#), [78](#)), but mechanisms by which dense liquid droplets transform to crystalline phases are largely unexplored.

Crystalline nanoparticles

Crystalline particles are distinct from the aforementioned precursor phases due to their ordered structure. Depending on symmetry, a crystal may have heterogeneous surface structure and distribution of surface charge, as well as a net dipole moment. Nanocrystals can possess the expected equilibrium morphologies or have rough surfaces and nonequilibrium shapes. Such morphological characteristics can substantially influence the particle-particle interactions that precede attachment, as well as the structure and microstructure of the resulting single crystals.

Atomic bonding, particle morphology, surface reconstruction, and particle size largely determine the structure of a nanoparticle. However, nanoparticle structure is not static; it changes in response to its environment, as demonstrated by ~ 3 -nm ZnS nanoparticles upon adsorption of water, organic molecules, and inorganic ions ([74](#), [80](#)). Similarly, nanoparticle structure is sensitive to aggregation state, as evidenced by the reversible ordering/disordering structural changes seen upon aggregation and disaggregation of small ZnS nanoparticles ([81](#)). In some cases, increasing size can result in decreased internal strain and defect content ([82](#)). Finally, in systems for which there is a switch in phase stability with particle size, as discussed above, nanoparticles of one phase may initially form and transform to the bulk phase as they aggregate and grow in size ([34](#), [56](#), [57](#), [60](#)). For example ~ 1 -nm ferrihydrite-like primary particles structurally rearrange upon attachment to the surface of magnetite crystals to merge with the magnetite crystal structure ([57](#)). In such systems, the structural differences may be accommodated if a match between the lattice planes of the two distinct phases can be achieved, as was reported for anatase and rutile TiO_2 ([60](#)), or may also result in disordered aggregates, as in the case of akaganéite assembly to form single-crystal hematite ([34](#)). However, after becoming part of the larger mass, the primary particles must transform to the bulk phase. If the interphase boundary is coherent, the

transformation can lead to the growth of branched single crystals; this may also result in twin boundaries or stacking faults at the branch sites (e.g., [Fig. 2G](#)). Alternatively, if the boundaries are incoherent, a single crystal can only result if recrystallization removes the boundaries, potentially obliterating any structural evidence of CPA ([34](#)).

Oligomers, polymers, and gels

In some systems, the monomers can form complexes or polymerize or aggregate into clusters before the formation of a new phase ([5](#), [28](#), [44](#), [68](#)). Consequently, the solution may contain a distribution of monomers, complexes, and clusters, all of which may play an active role in nucleation and growth, complicating identification of one species as the fundamental unit. Alternatively, all but one of the observed species may be spectators, with the active species being consumed as quickly as they are produced. Thus, detectable species may not substantially contribute to nucleation and growth. If, for dynamical reasons, complex species form interconnected networks, they may create a dynamically arrested gel state, which only crystallizes upon heating ([Fig. 4E](#)) ([83](#)).

The dynamics of postnucleation growth by monomers and particles

After the nucleation stage, the newly formed phases grow and coarsen, potentially via many competing processes ([Fig. 5](#)). Whether or not CPA dominates over monomer addition depends on numerous factors associated with both the free-energy landscape and the kinetics of the system.

- [Download high-res image](#)
- [Open in new tab](#)
- [Download Powerpoint](#)

Fig. 5 Multiple growth mechanisms can occur simultaneously within a single crystallizing system, depending on the values of global parameters such as supersaturation, local factors that include interface curvature, and materials parameters such as phase stability versus particle size.

(A) In this diagram, the arrows indicate the direction of motion of monomers, clusters, or surfaces, and the dashed lines give the crystallographic orientations of nanocrystals. The expanded oval shows molecular-scale processes. OR, Ostwald ripening; MA, molecular attachment; CA, cluster attachment; A, amorphous addition; OA, oriented attachment; NOA, non- or

semi-oriented attachment; RC, recrystallization. The phases are denoted by uniform blue for an amorphous crystal, wavy lines for a poorly ordered crystal, and solid lines for a well-ordered crystal. **(B)** Twins, stacking faults, and dislocations can result from the attachment of crystalline particles.

The extent to which monomers participate in the postnucleation stage depends on the relative rates of attachment and detachment. When surfaces are atomically rough, the growth rate is controlled by diffusion. For faceted interfaces, the attachment and detachment rates depend on the kink site density and the energy to create new kinks ([84](#)). In both limits, the theory of growth is well developed ([84](#)).

Conventional understanding of particle-particle interactions relies on the theory of Derjaguin, Landau, Verwey, and Overbeek (DLVO) for colloidal particles that are typically much larger than the nanoparticles involved in crystal growth ([85](#), [86](#)). Classical DLVO theory considers the surface charge repulsion and the van der Waals interaction between two particles, with many simplifications in the mathematical derivation. Although successful in interpreting some observations of colloids, DLVO theory is unable to predict the orientation dependence of nanoparticle growth via OA. This is attributed in part to non-DLVO forces, such as solvation, and the omission of Coulombic interactions between interacting particles. For inorganic nanoparticles in close proximity, Coulombic and Lewis acid/base interactions predominate over van der Waals interactions and random Brownian forces, thereby guiding the interacting particles to find energetically favorable crystallographic orientations for attachment ([87-89](#)). Molecular energetic calculations predicted preferred attachment surfaces and crystal growth orientations for more than 30 crystals that largely agree with experimental results ([88](#)), demonstrating the importance of Coulomb interactions during OA ([29](#), [61](#)).

Because monomer attachment rates scale with solubility, it is arguably the most important parameter determining relative contributions of monomer-by-monomer addition or addition of nanoparticles. For example, as the solubility drops from molar levels to submicromolar levels, at equivalent values of supersaturation the rates of monomer addition drop by a factor of $\sim 10^{10}$ ([90](#)). However, the translational and rotational diffusivity of particles is strongly attenuated by particle size, varying as R^{-1} and R^{-3} , respectively. Because critical nucleus size also increases with increasing solubility, these strong dependencies again reduce the likelihood that CPA dominates at high solubility.

Even when CPA dominates, crystallization is unlikely to proceed without the concurrent process of Ostwald ripening ([Fig. 5](#)) ([28](#)). This is because particle solubility increases as the radius decreases via the Gibbs-Thomson relation ([41](#)). Both attached and dispersed particles with radii of curvature smaller than the ensemble average will tend to dissolve, whereas those with larger

radii will grow. Therefore, the competition between monomer-by-monomer growth and growth by attachment of particles of different sizes must be considered. In poorly mixed systems, the local curvature of nearby particles can determine this competition. For example, although small particles near highly curved regions of larger ones may aggregate with little competition from Ostwald ripening, those near flat or negatively curved regions may rapidly dissolve, resulting in net transfer of monomers to the larger mass (34).

Because initial nucleation from solution most often produces a polydisperse population of nanoparticles, their assembly typically leads to irregular crystal morphology with protrusions, branches, and pores. The extent and pattern of these structures depends on the degree to which monomer attachment and detachment is rapid enough to smoothen the interface, filling regions of negative curvature formed by attachment events. Therefore, the development of experimental model systems, simulations, and ultimately a theory that predicts growth shape, kinetics, crystallinity, and the resulting defect structure depends on an ability to account for the competing contribution of monomers and particles to postnucleation growth and coarsening.

Effect of extrinsic factors: Surfaces, impurities, and confinement

The presence of a foreign surface in a crystallizing system can dramatically alter the pathway of crystallization for the simple reason that barriers to nucleation can be lowered due to a reduction in the interfacial free energy (3, 44). In the case of calcite, the rate of heterogeneous nucleation on functionalized surfaces has been predicted to be 20 orders of magnitude higher than that of homogeneous nucleation (3, 73). A similar result was found for calcium phosphate nucleation on collagen (5). Consequently, although pathways via precursor phases and particle aggregation may dominate in a system free of preexisting interfaces, the presence of an interface can redirect the nucleation pathway toward the classical monomer-by-monomer process at low supersaturation.

A more complex situation exists for monomers confined in restricted volumes—for example, in crevices and small pores (91, 92). Where the pore surface is wetted by the nucleus, nucleation rates should be enhanced over those on flat substrates for pore dimensions on the order of the critical nucleus size, because the curvature of the pore enables a larger fraction of the nucleus to be in contact with the substrate. However, dramatic effects on the stability of metastable phases within confined volumes that are orders of magnitude larger than the length scale expected for the critical nucleus have been reported for solutions confined between crossed cylinders (71, 93) and in

liposomes ([72](#), [94](#)). [The latter may be representative of sea urchin embryos ([95](#)).] Possible factors to which the observed stabilization was attributed include statistical effects associated with small volumes and low probabilities for nucleating the stable phases, exclusion of heterogeneous nucleators, restriction of the mobility and presence of water, lack of contact with the solution phase required for transformation, and/or an inability to aggregate into larger particles for which the bulk phase has greater stability. Moreover, solute and solvent activities, ion mobilities, and ion distributions—and thus interfacial free energy and supersaturation—are all likely to depend on pore size and the nature of the pore surface for sufficiently small pores. Thus, the effect of confinement on nucleation pathways and rates is only beginning to be understood.

Organic molecules in solution can also affect pathways and rates of crystal formation. Additives (e.g., polymers and surfactants) that colloidally stabilize nanoparticles are believed to promote nanoparticle assembly into superlattices and mesocrystals ([6](#), [39](#), [96](#)), with stabilizing ligands residing at the nanoparticle interfaces ([37](#)), although recent investigations highlight the difficulty in determining whether a crystal possesses the attributes of a mesocrystal ([33](#)). Several mechanisms of nanoparticle alignment by organics have been proposed, including directed nucleation or attachment in a prealigned organic matrix ([9](#)), such as collagen ([97](#)) or chitin, or alignment through physical interactions ([9](#), [38](#)).

Organics have also been shown to modulate the kinetics of inorganic nucleation and growth. In fact, macromolecules, particularly those that are acidic such as polyacrylic acid and aspartic and glutamic acid-rich (poly)peptides and proteins, can dramatically increase induction times ([98](#)), stabilize amorphous precursors ([97](#), [99](#)), induce formation of dense liquid phases ([21](#), [100](#)), and modify crystal size and shape ([101](#)) in vitro. Several soluble proteins in biomineral systems are presumed to have similar effects in natural systems, although there are very few biomineral proteins whose function in vivo has been clearly identified, and most proposed functions are primarily based on in vitro observations ([102–105](#)).

Both inorganic and organic additives can play key roles in determining the structural pathways of nucleation and growth in systems where the final crystal structure consists of an open framework (e.g., zeolites). The use of organic or inorganic species as structure-directing agents (SDAs) is a common method to facilitate the formation of microporous materials. In the case of organic SDAs ([106](#)), their size and structure tend to be commensurate with the pores and/or channels of the structures they direct. The organic is often occluded within the pores of the crystal as it grows, and there is good evidence that the building blocks are complex units consisting of either disordered particles that order upon addition to the framework or preformed oligomeric units of the framework ([Fig. 5](#)). Whether these SDAs

simply promote the kinetics of certain molecular assembly pathways or create local minima in the free-energy landscape remains unknown.

Challenges and directions for the future

Although geological materials provided early examples of CPA ([107](#)), efforts to establish the scope of this process in natural environments have barely begun. Particle-based mineral formation may have particular importance for the biogeochemical cycling of nutrients and metals, as well as environmental remediation. The environmental mineral phases involved in elemental uptake and release, such as the iron oxides, are aggregates of primary units whose metal sorption, encapsulation, and release properties are highly size dependent ([58](#), [59](#)). Furthermore, climate reconstructions are based upon the chemical and morphological characteristics of biological and inorganic minerals in the sedimentary record. In addition to a better understanding of the origins and evolution of skeletal structures, particle-based pathways may finally explain the enigmatic textures and compositions of carbonate deposits that formed as Earth transitioned from an inorganic to a biological world ([8](#), [108](#)). Interpreting the patterns in these ancient materials, however, will present multiple challenges because the pathway from precursor particles to final stable phase occurred millions (or even billions) of years in the past.

A predictive understanding of CPA also promises advances in nanomaterials design and synthesis for diverse applications. This mechanism of crystallization is believed to dominate solution-based growth of important semiconductor, oxide, and metallic nanoparticles, such as TiO_2 , Fe_2O_3 , CeO_2 , ZnO , SnO_2 , CdSe , PbSe , ZnS , PbS , Cu_7Te_4 , Bi_2Te_3 , Au , Ag , Pt , and Pt_3Fe ([60](#), [88](#), [109](#)), and can be exploited to produce hierarchical structures that retain the size-dependent properties of the nanoscale building blocks ([96](#)). The branched nanomaterials that can result from CPA ([Fig. 2G](#)) are of particular interest because they can have short electron mean free paths ([110](#)), large photon absorption cross sections ([111](#)), and complex patterns of optical scattering ([112](#)), all of which can improve photovoltaic and photocatalytic efficiency.

Similarly, the nanoparticle architecture of mesocrystals and superlattices ([Fig. 2H](#)) results in enhanced or novel thermoelectric, photonic, catalytic, and photovoltaic properties ([113](#)). The intrinsically anisotropic directional properties of the nanoparticle building blocks should promote directional amplification of physical properties and fields. Open framework materials like zeolites ([Fig. 2, I and J](#)) and metal organic framework compounds, some of which are known to be formed by CPA ([114](#)), exhibit pore dimensions and geometries well suited to CO_2 capture, H_2 storage, emissions control, catalysis for biomass conversion, and molecular separation for refrigerant-free dehumidification and biofuel purification ([115](#)).

For natural and synthetic materials alike, efforts to decipher signals from preexisting particles will require an understanding of mineralization from both forward and reverse perspectives. That is, direct observations and simulations of crystals that are developing by particle-mediated mechanisms will provide mechanistic insights into formation processes, and parallel studies that revisit the structure and composition of preexisting crystals will be needed to critically reevaluate long-standing assumptions about the conditions of their formation.

Despite the numerous implications of CPA in diverse systems, many knowledge gaps remain. We do not understand the structure of solvent and ions at solid-solution interfaces, nor how this structure evolves as a function of interparticle separation (**Fig. 6**). The fields and forces at these interfaces, their scaling as assembly proceeds, and their translation into particle motions are unknown. The nanoscale physics and chemistry operating within the interfacial region between particles that govern alignment and attachment events are poorly understood, as is the size dependence of surface energy, solvation energy, and phase stability. Moreover, a complete picture of crystallization must include classical monomer-by-monomer dissolution, precipitation, and ripening, which are convolved in space and time with the dynamics of particle motion, collision, and aggregation (**Fig. 5**). Given the inherent feedback between the dynamics of solvent and ion distributions in the interfacial region and the motion of particles, a predictive description must cross scales to seamlessly connect molecular details with ensemble behavior. Thus, although models of particle interactions and aggregation in simple colloidal systems are mature, they cannot describe CPA due to the complexities of energy landscapes and anisotropies in shape, atomic structure, surface charge, and adsorbate coverage, as well as the dynamic nature of dense liquid, gel, and amorphous particles.

- [Download high-res image](#)
- [Open in new tab](#)
- [Download Powerpoint](#)

Fig. 6 Major gaps remain in the understanding of CPA.

Nanoparticle assembly is influenced by the structure of solvent and ions at solid-solution interfaces and confined regions of solution between solid surfaces. The details of solution and solid structure create the set of forces that drive particle motion. However, as the particles move, the local structure and the corresponding forces change, taking the particles from a regime of long-range to short-range interactions and eventually leading to particle-attachment events.

To address these knowledge gaps, in situ measurements will be critical. Powerful new experimental approaches based on x-ray spectroscopy and scattering, electron microscopy, and scanning probe methods hold promise for exploring the dynamics of CPA. When combined with emerging molecular-to-mesoscale modeling techniques, these methods promise to reveal new insights into the nature of the interface, the source of the forces driving aggregation, the role of solvation, and the dynamics of particle movement, alignment, and attachment. To exploit these new tools, an important challenge is to identify crystal systems that are amenable to a combination of techniques to facilitate comprehensive morphological and structural characterization of crystallization pathways.

Looking ahead, a multidisciplinary effort will be required to decipher the complexity of particle-attachment pathways. Only through integrative approaches will a molecular and quantitative understanding emerge that is comparable to the classical nucleation and growth theories that advanced our understanding over the past 50 years. A complete physical picture of crystallization that encompasses the diversity of potential pathways must now be developed if the many scientific fields in which crystallization is a common phenomenon are to reach their full potential.

Note added in proof: During the development of this article, a review of oriented attachment was published by Ivanov *et al.* ([120](#)).

- [↩](#)* Previously publishing as Gelsomina De Stasio.

References and Notes

1. [↩](#)

1. D. Kashchiev

, Thermodynamically consistent description of the work to form a nucleus of any size. *J. Chem. Phys.* **118**, 1837–1851 (2003). [10.1063/1.1531614](https://doi.org/10.1063/1.1531614)[doi:10.1063/1.1531614](https://doi.org/10.1063/1.1531614)

ACCESS PROVIDED BY
 [UC-eLinks](#)[CrossRef](#)[Google Scholar](#)

2. [↩](#)

1. W. K. Burton,

2. N. Cabrera,

3. F. C. Frank

, The growth of crystals and the equilibrium structure of their surfaces. *Philos. Trans. R. Soc. Lond. A* **243**, 299–358 (1951).10.1098/rsta.1951.0006doi:10.1098/rsta.1951.0006

Accessed by



[UC-eLinks](#)[Abstract](#)/[FREE Full Text](#)[Google Scholar](#)

3. [↩](#)

1. A. J. Giuffre,
2. L. M. Hamm,
3. N. Han,
4. J. J. De Yoreo,
5. P. M. Dove

, Polysaccharide chemistry regulates kinetics of calcite nucleation through competition of interfacial energies. *Proc. Natl. Acad. Sci. U.S.A.* **110**,9261–9266 (2013). 10.1073/pnas.1222162110pmid:23690577 doi:10.1073/pnas.1222162110

Accessed by



[UC-eLinks](#)[Abstract](#)/[FREE Full Text](#)[Google Scholar](#)

4. [↩](#)

1. D. N. Petsev,
2. K. Chen,
3. O. Gliko,
4. P. G. Vekilov

, Diffusion-limited kinetics of the solution-solid phase transition of molecular substances. *Proc. Natl. Acad. Sci. U.S.A.* **100**, 792–796 (2003).10.1073/pnas.0333065100pmid:12552115 doi:10.1073/pnas.0333065100

Accessed by



[UC-eLinks](#)[Abstract](#)/[FREE Full Text](#)[Google Scholar](#)

5. [↩](#)

1. W. J. Habraken,
2. J. Tao,
3. L. J. Brylka,
4. H. Friedrich,
5. L. Bertinetti,

6. A. S. Schenk,
7. A. Verch,
8. V. Dmitrovic,
9. P. H. H. Bomans,
10. P. M. Frederik,
11. J. Laven,
12. P. van der Schoot,
13. B. Aichmayer,
14. G. de With,
15. J. J. DeYoreo,
16. N. A. Sommerdijk


, Ion-association complexes unite classical and non-classical theories for the biomimetic nucleation of calcium phosphate. *Nat. Commun.* **4**, 1507 (2013). 10.1038/ncomms2490pmid:23422675doi:10.1038/ncomms2490

ACCESSible BY
 [UC-eLinks](#)[CrossRef](#)[PubMed](#)[Google Scholar](#)

6. [↩](#)

1. K. S. Cho,
2. D. V. Talapin,
3. W. Gaschler,
4. C. B. Murray

, Designing PbSe nanowires and nanorings through oriented attachment of nanoparticles. *J. Am. Chem. Soc.* **127**, 7140-7147 (2005).10.1021/ja050107spmid:15884956 doi:10.1021/ja050107

S
ACCESSible BY
 [UC-eLinks](#)[CrossRef](#)[PubMed](#)[Web of Science](#)[Google Scholar](#)

7. [↩](#)

H. A. Lowenstam, S. Weiner, *On Biomineralization* (Oxford Univ. Press, New York, 1989).

[Google Scholar](#)

8. [↩](#)

J. P. Grotzinger, N. P. James, in *Carbonate Sedimentation and Diagenesis in the Evolving Precambrian World* (Society for Sedimentary Geology, Tulsa, OK, 2000), vol. 67, pp. 3–20.

[Google Scholar](#)

9. [↩](#)

H. Cölfen, M. Antonietti, *Mesocrystals and Nonclassical Crystallization* (Wiley, Chichester, England; Hoboken, NJ, 2008).

[Google Scholar](#)

10. [↩](#)

E. Beniash, J. Aizenberg, L. Addadi, S. Weiner, Amorphous calcium carbonate transforms into calcite during sea urchin larval spicule growth. *Proc. R. Soc. B-Biol. Sci.* **264**, 461–465 (1997).

[Google Scholar](#)

11. [↩](#)

1. Y. U. T. Gong,
2. C. E. Killian,
3. I. C. Olson,
4. N. P. Appathurai,
5. A. L. Amasino,
6. M. C. Martin,
7. L. J. Holt,
8. F. H. Wilt,
9. P. U. P. A. Gilbert

, Phase transitions in biogenic amorphous calcium carbonate. *Proc. Natl. Acad. Sci. U.S.A.* **109**, 6088–6093 (2012). 10.1073/pnas.1118085109pmid:22492931 doi:10.1073/pnas.1118085109

ACCESSible BY

Library

[UC-eLinks](#)[Abstract/FREE Full Text](#)[Google Scholar](#)

12. [↩](#)

1. Y. Politi,
2. T. Arad,
3. E. Klein,

4. S. Weiner,
5. L. Addadi

, Sea urchin spine calcite forms via a transient amorphous calcium carbonate phase. *Science* **306**, 1161-1164 (2004). 10.1126/science.1102289pmid:15539597doi:10.1126/science.1102289

ACCESS PROVIDED BY



[UC-eLinks](#)[Abstract](#)/[FREE Full Text](#)[Google Scholar](#)

13. [↵](#)

1. C. E. Killian,
2. R. A. Metzler,
3. Y. U. T. Gong,
4. I. C. Olson,
5. J. Aizenberg,
6. Y. Politi,
7. F. H. Wilt,
8. A. Scholl,
9. A. Young,
10. A. Doran,
11. M. Kunz,
12. N. Tamura,
13. S. N. Coppersmith,
14. P. U. P. A. Gilbert

, Mechanism of calcite co-orientation in the sea urchin tooth. *J. Am. Chem. Soc.* **131**, 18404-18409 (2009). 10.1021/ja907063zpmid:19954232doi:10.1021/ja907063z

ACCESS PROVIDED BY



[UC-eLinks](#)[CrossRef](#)[PubMed](#)[Web of Science](#)[Google Scholar](#)

14. [↵](#)

1. E. Beniash,
2. R. A. Metzler,
3. R. S. K. Lam,
4. P. U. P. A. Gilbert

, Transient amorphous calcium phosphate in forming enamel. *J. Struct. Biol.* **166**, 133–143 (2009). 10.1016/j.jsb.2009.02.001pmid:19217943doi:10.1016/j.jsb.2009.02.001

ACCESS FULL BY



[UC-eLinks](#)[CrossRef](#)[PubMed](#)[Web of Science](#)[Google Scholar](#)

15. [↵](#)

1. J. Mahamid,
2. A. Sharir,
3. L. Addadi,
4. S. Weiner

, Amorphous calcium phosphate is a major component of the forming fin bones of zebrafish: Indications for an amorphous precursor phase. *Proc. Natl. Acad. Sci. U.S.A.* **105**, 12748–12753 (2008). 10.1073/pnas.0803354105pmid:18753619 doi:10.1073/pnas.0803354105

ACCESS FULL BY



[UC-eLinks](#)[Abstract/FREE Full Text](#)[Google Scholar](#)

16. [↵](#)

1. R. Dillaman,
2. S. Hequembourg,
3. M. Gay

, Early pattern of calcification in the dorsal carapace of the blue crab, *Callinectes sapidus*. *J. Morphol.* **263**, 356–374 (2005). 10.1002/jmor.10311pmid:15688443doi:10.1002/jmor.10311

ACCESS FULL BY



[UC-eLinks](#)[CrossRef](#)[PubMed](#)[Web of Science](#)[Google Scholar](#)

17. [↵](#)

1. L. Gago-Duport,
2. M. J. I. Briones,
3. J. B. Rodríguez,
4. B. Covelo

, Amorphous calcium carbonate biomineralization in the earthworm's calciferous gland: Pathways to the formation of crystalline phases. *J. Struct. Biol.* **162**, 422–

435 (2008). 10.1016/j.jsb.2008.02.007pmid:18400515doi:10.1016/j.jsb.2008.02.007

ACCESS FULL BY



[UC-eLinks](#)[CrossRef](#)[PubMed](#)[Web of Science](#)[Google Scholar](#)

18. [↵](#)

1. I. M. Weiss,
2. N. Tuross,
3. L. Addadi,
4. S. Weiner

, Mollusc larval shell formation: Amorphous calcium carbonate is a precursor phase for aragonite. *J. Exp. Zool.* **293**, 478–491 (2002).10.1002/jez.90004pmid:12486808 doi:10.1002/jez.90004

ACCESS FULL BY



[UC-eLinks](#)[CrossRef](#)[PubMed](#)[Web of Science](#)[Google Scholar](#)

19. [↵](#)

1. K. M. Towe,
2. H. A. Lowenstam

, Ultrastructure and development of iron mineralization in the radular teeth of *Cryptochiton stelleri* (mollusca). *J. Ultrastruct. Res.* **17**, 1–13 (1967). 10.1016/S0022-5320(67)80015-7pmid:6017357 doi:10.1016/S0022-5320(67)80015-7

ACCESS FULL BY



[UC-eLinks](#)[CrossRef](#)[PubMed](#)[Web of Science](#)[Google Scholar](#)

20. [↵](#)

1. S. L. Burkett,
2. M. E. Davis

, Mechanism of structure direction in the synthesis of Si-ZSM-5: An investigation by intermolecular ^1H - ^{29}Si CP MAS NMR. *J. Phys. Chem.* **98**, 4647–4653 (1994).10.1021/j100068a027doi:10.1021/j100068a027

ACCESS FULL BY



[UC-eLinks](#)[CrossRef](#)[Web of Science](#)[Google Scholar](#)

21. [↵](#)

1. L. B. Gower,

2. D. J. Odom
, Deposition of calcium carbonate films by a polymer-induced liquid-precursor (PILP) process. *J. Cryst. Growth* **210**, 719–734 (2000).
10.1016/S0022-0248(99)00749-6doi:10.1016/S0022-0248(99)00749-6

Access provided by



[UC-eLinks](#)[CrossRef](#)[Web of Science](#)[Google Scholar](#)

22. [↩](#)

1. R. L. Penn,
2. J. F. Banfield
, Imperfect oriented attachment: Dislocation generation in defect-free nanocrystals. *Science* **281**, 969–971 (1998). 10.1126/science.281.5379.969pmid:9703506doi:10.1126/science.281.5379.969

Access provided by



[UC-eLinks](#)[Abstract/FREE Full Text](#)[Google Scholar](#)

23. [↩](#)

1. M. Li,
2. H. Schnablegger,
3. S. Mann
, Coupled synthesis and self-assembly of nanoparticles to give structures with controlled organization. *Nature* **402**, 393–395 (1999). 10.1038/46509doi:10.1038/46509

Access provided by



[UC-eLinks](#)[CrossRef](#)[Web of Science](#)[Google Scholar](#)

24. [↩](#)

1. D. Schwahn,
2. Y. R. Ma,
3. H. Cölfen
, Mesocrystal to single crystal transformation of D,L-alanine evidenced by small angle neutron scattering. *J. Phys. Chem. C* **111**, 3224–3227 (2007).10.1021/jp068813doi:10.1021/jp068813i

Access provided by



[UC-eLinks](#)[CrossRef](#)[Web of Science](#)[Google Scholar](#)

25. [↩](#)

1. P.-A. Fang,

2. J. F. Conway,
3. H. C. Margolis,
4. J. P. Simmer,
5. E. Beniash

, Hierarchical self-assembly of amelogenin and the regulation of biomineralization at the nanoscale. Proc. Natl. Acad. Sci. U.S.A. **108**,14097–14102 (2011). 10.1073/pnas.1106228108pmid:21825148 doi:10.1073/pnas.1106228108

ACCESSible BY



[UC-eLinks](#)[Abstract](#)/[FREE Full Text](#)[Google Scholar](#)

26. [↵](#)

1. R. Demichelis,
2. P. Raiteri,
3. J. D. Gale,
4. D. Quigley,
5. D. Gebauer

, Stable prenucleation mineral clusters are liquid-like ionic polymers. Nat. Commun. **2**, 590 (2011). 10.1038/ncomms1604pmid:22186886doi:10.1038/ncomms1604

ACCESSible BY



[UC-eLinks](#)[CrossRef](#)[PubMed](#)[Google Scholar](#)

27. [↵](#)

1. D. Li,
2. M. H. Nielsen,
3. J. R. I. Lee,
4. C. Frandsen,
5. J. F. Banfield,
6. J. J. De Yoreo

, Direction-specific interactions control crystal growth by oriented attachment. Science **336**, 1014–1018 (2012).10.1126/science.1219643 pmid:22628650 doi:10.1126/science.1219643

ACCESSible BY



[UC-eLinks](#)[Abstract](#)/[FREE Full Text](#)[Google Scholar](#)

28. [↵](#)

1. A. I. Lupulescu,
2. J. D. Rimer

, In situ imaging of silicalite-1 surface growth reveals the mechanism of crystallization. *Science* **344**, 729–732 (2014). 10.1126/science.1250984
pmid:24833388doi:10.1126/science.1250984

Access provided by



[UC-eLinks](#)[Abstract/FREE Full Text](#)[Google Scholar](#)

29. [↵](#)

1. Q. Chen,
2. H. Cho,
3. K. Manthiram,
4. M. Yoshida,
5. X. Ye,
6. A. P. Alivisatos

, Interaction potentials of anisotropic nanocrystals from the trajectory sampling of particle motion using in situ liquid phase transmission electron microscopy. *ACS Cent. Sci.* **1**, 33– 39 (2015).10.1021/acscentsci.5b00001doi:10.1021/acscentsci.5b00001

Access provided by



[UC-eLinks](#)[CrossRef](#)[Google Scholar](#)

30. [↵](#)

1. M. H. Nielsen,
2. S. Aloni,
3. J. J. De Yoreo

, In situ TEM imaging of CaCO₃ nucleation reveals coexistence of direct and indirect pathways. *Science* **345**, 1158–1162 (2014). 25190792pmid:25190792

Access provided by



[UC-eLinks](#)[Abstract/FREE Full Text](#)[Google Scholar](#)

31. [↵](#)

1. K. K. Sand,
2. J. D. Rodriguez-Blanco,

3. E. Makovicky,
4. L. G. Benning,
5. S. L. S. Stipp

, Crystallization of CaCO₃ in water-alcohol mixtures: Spherulitic growth, polymorph stabilization, and morphology change. Cryst. Growth Des. **12**, 842–853 (2012). 10.1021/cg2012342doi:10.1021/cg2012342

ACCESS FULLY BY



[UC-eLinks](#)[CrossRef](#)[Google Scholar](#)

32. [↩](#)

1. F. C. Meldrum,
2. S. Ludwigs

, Template-directed control of crystal morphologies. Macromol. Biosci. **7**, 152–162 (2007). 10.1002/mabi.200600191pmid:17295402 doi:10.1002/mabi.200600191

ACCESS FULLY BY



[UC-eLinks](#)[CrossRef](#)[PubMed](#)[Google Scholar](#)

33. [↩](#)

1. Y. Y. Kim,
2. A. S. Schenk,
3. J. Ihli,
4. A. N. Kulak,
5. N. B. J. Hetherington,
6. C. C. Tang,
7. W. W. Schmahl,
8. E. Griesshaber,
9. G. Hyett,
10. F. C. Meldrum

, A critical analysis of calcium carbonate mesocrystals. Nat. Commun. **5**, 4341 (2014). 25014563pmid:25014563

ACCESS FULLY BY



[UC-eLinks](#)[PubMed](#)[Google Scholar](#)

34. [↩](#)

1. M. H. Nielsen,

2. D. Li,
3. H. Zhang,
4. S. Aloni,
5. T. Y. J. Han,
6. C. Frandsen,
7. J. Seto,
8. J. F. Banfield,
9. H. Cölfen,
10. J. J. De Yoreo

, Investigating processes of nanocrystal formation and transformation via liquid cell TEM. *Microsc. Microanal.* **20**, 425–436 (2014). 10.1017/S1431927614000294pmid:24625923doi:10.1017/S1431927614000294



35. [↩](#)

1. N. D. Burrows,
2. C. R. H. Hale,
3. R. L. Penn

, Effect of pH on the kinetics of crystal growth by oriented aggregation. *Cryst. Growth Des.* **13**, 3396–3403 (2013). 10.1021/cg4001939doi:10.1021/cg4001939



36. [↩](#)

1. A. Gal,
2. K. Kahil,
3. N. Vidavsky,
4. R. T. DeVol,
5. P. U. P. A. Gilbert,
6. P. Fratzl,
7. S. Weiner,
8. L. Addadi

, Particle accretion mechanism underlies biological crystal growth from an amorphous precursor phase. *Adv. Funct. Mater.* **24**, 5420–5426 (2014). 10.1002/adfm.201400676doi:10.1002/adfm.201400676

Accessed by



[UC-eLinks](#)[CrossRef](#)[Google Scholar](#)

37. [↩](#)

1. H. Cölfen,
2. M. Antonietti

, Mesocrystals: Inorganic superstructures made by highly parallel crystallization and controlled alignment. *Angew. Chem. Int. Ed.* **44**, 5576–5591 (2005).10.1002/anie.200500496pmid:16035009 doi:10.1002/anie.200500496

Accessed by



[UC-eLinks](#)[CrossRef](#)[PubMed](#)[Web of Science](#)[Google Scholar](#)

38. [↩](#)

1. R. Q. Song,
2. H. Cölfen

, Mesocrystals: Ordered nanoparticle superstructures. *Adv. Mater.* **22**, 1301–1330(2010). 10.1002/adma.200901365pmid:20437477 doi:10.1002/adma.200901365

Accessed by




[UC-eLinks](#)[CrossRef](#)[PubMed](#)[Google Scholar](#)

39. [↩](#)

1. M. P. Boneschanscher,
2. W. H. Evers,
3. J. J. Geuchies,
4. T. Altantzis,
5. B. Goris,
6. F. T. Rabouw,
7. S. A. P. van Rossum,
8. H. S. J. van der Zant,
9. L. D. A. Siebbeles,
10. G. Van Tendeloo,
11. I. Swart,

12. J. Hilhorst,
13. A. V. Petukhov,
14. S. Bals,
15. D. Vanmaekelbergh


, Long-range orientation and atomic attachment of nanocrystals in 2D honeycomb superlattices. *Science* **344**, 1377-1380 (2014). 10.1126/science.1252642pmid:24948734doi:10.1126/science.1252642

ACCESSible BY
 [UC-eLinksAbstract/FREE Full TextGoogle Scholar](#)

40. [↵](#)

1. A. F. Wallace,
2. L. O. Hedges,
3. A. Fernandez-Martinez,
4. P. Raiteri,
5. J. D. Gale,
6. G. A. Waychunas,
7. S. Whitelam,
8. J. F. Banfield,
9. J. J. De Yoreo


, Microscopic evidence for liquid-liquid separation in supersaturated CaCO_3 solutions. *Science* **341**, 885-889 (2013). 10.1126/science.1230915pmid:23970697doi:10.1126/science.1230915

ACCESSible BY
 [UC-eLinksAbstract/FREE Full TextGoogle Scholar](#)

41. [↵](#)

1. P. W. Voorhees

, The theory of Ostwald ripening. *J. Stat. Phys.* **38**, 231-252 (1985).10.1007/BF01017860doi:10.1007/BF01017860

ACCESSible BY
 [UC-eLinksCrossRefGoogle Scholar](#)

42. [↵](#)

1. A. J. Bray

, Theory of phase-ordering kinetics. *Adv. Phys.* **51**, 481–587 (2002).10.1080/00018730110117433doi:10.1080/00018730110117433

Access provided by



[UC-eLinks](#)[CrossRef](#)[Web of Science](#)[Google Scholar](#)

43. [↶](#)

1. B. Scheifele,
2. I. Saika-Voivod,
3. R. K. Bowles,
4. P. H. Poole

, Heterogeneous nucleation in the low-barrier regime. *Phys. Rev. E Stat. Nonlin. Soft Matter*

Phys. **87**, 042407 (2013).10.1103/PhysRevE.87.042407pmid:23679429doi:10.1103/PhysRevE.87.042407

Access provided by



[UC-eLinks](#)[CrossRef](#)[PubMed](#)[Google Scholar](#)

44. [↶](#)

1. A. Dey,
2. P. H. H. Bomans,
3. F. A. Müller,
4. J. Will,
5. P. M. Frederik,
6. G. de With,
7. N. A. Sommerdijk

, The role of prenucleation clusters in surface-induced calcium phosphate crystallization. *Nat. Mater.* **9**, 1010–1014(2010). 10.1038/nmat2900pmid:21076415 doi:10.1038/nmat2900

Access provided by



[UC-eLinks](#)[CrossRef](#)[PubMed](#)[Web of Science](#)[Google Scholar](#)

45. [↶](#)

P. T. Cardew, R. J. Davey, The kinetics of solvent-mediated phase-transformations. *Proc. R. Soc. London Ser. A-Math. Phys. Eng. Sci.* **398**, 415–428 (1985).

[Google Scholar](#)

46. [↵](#)

1. T. Y. J. Han,
2. J. Aizenberg

, Calcium carbonate storage in amorphous form and its template-induced crystallization. *Chem. Mater.* **20**, 1064–1068 (2008). 10.1021/cm702032vdoi:10.1021/cm702032v

ACCESS FULL BY



[UC-eLinks](#)[CrossRef](#)[Web of Science](#)[Google Scholar](#)

47. [↵](#)

1. E. M. Pouget,
2. P. H. H. Bomans,
3. J. A. Goos,
4. P. M. Frederik,
5. G. de With,
6. N. A. Sommerdijk

, The initial stages of template-controlled CaCO₃ formation revealed by cryo-TEM. *Science* **323**, 1455–1458 (2009).10.1126/science.1169434p mid:19286549 doi:10.1126/science.1169434

ACCESS FULL BY



[UC-eLinks](#)[Abstract/FREE Full Text](#)[Google Scholar](#)

48. [↵](#)

1. A. Gal,
2. W. Habraken,
3. D. Gur,
4. P. Fratzl,
5. S. Weiner,
6. L. Addadi

, Calcite crystal growth by a solid-state transformation of stabilized amorphous calcium carbonate nanospheres in a hydrogel. *Angew. Chem. Int. Ed.* **52**, 4867–4870 (2013). 10.1002/anie.201210329pmid:23559356 doi:10.1002/anie.201210329

ACCESS FULL BY



[UC-eLinks](#)[CrossRef](#)[PubMed](#)[Web of Science](#)[Google Scholar](#)

49. [↶](#)

1. O. Galkin,
2. K. Chen,
3. R. L. Nagel,
4. R. E. Hirsch,
5. P. G. Vekilov

, Liquid-liquid separation in solutions of normal and sickle cell hemoglobin. Proc. Natl. Acad. Sci. U.S.A. **99**, 8479-8483 (2002).10.1073/pnas.122055299pmid:12070342 doi:10.1073/pnas.122055299

UC LIBRARY

BERKELEY
Library
UNIVERSITY OF CALIFORNIA

[UC-eLinks](#)[Abstract/FREE Full Text](#)[Google Scholar](#)

50. [↶](#)

1. X. L. Wang,
2. I. M. Chou,
3. W. X. Hu,
4. R. C. Burruss

, In situ observations of liquid-liquid phase separation in aqueous MgSO₄ solutions: Geological and geochemical implications. Geochim. Cosmochim. Acta **103**, 1-10 (2013). 10.1016/j.gca.2012.10.044doi:10.1016/j.gca.2012.10.044

UC LIBRARY

BERKELEY
Library
UNIVERSITY OF CALIFORNIA

[UC-eLinks](#)[CrossRef](#)[Google Scholar](#)

51. [↶](#)

1. P. R. ten Wolde,
2. D. Frenkel

, Enhancement of protein crystal nucleation by critical density fluctuations. Science **277**, 1975-1978 (1997). 10.1126/science.277.5334.1975pmid:9302288doi:10.1126/science.277.5334.1975

UC LIBRARY

BERKELEY
Library
UNIVERSITY OF CALIFORNIA

[UC-eLinks](#)[Abstract/FREE Full Text](#)[Google Scholar](#)

52. [↶](#)

1. S. E. Wolf,
2. J. Leiterer,

3. M. Kappl,
4. F. Emmerling,
5. W. Tremel

, Early homogenous amorphous precursor stages of calcium carbonate and subsequent crystal growth in levitated droplets. *J. Am. Chem. Soc.* **130**,12342-12347 (2008). 10.1021/ja800984ypmid:18717561 doi:10.1021/ja800984y

Accessed by



[UC-eLinks](#)[CrossRef](#)[PubMed](#)[Web of Science](#)[Google Scholar](#)

53. [↩](#)

1. M. A. Bewernitz,
2. D. Gebauer,
3. J. Long,
4. H. Cölfen,
5. L. B. Gower

, A metastable liquid precursor phase of calcium carbonate and its interactions with polyaspartate. *Faraday Discuss.* **159**, 291-312 (2012).10.1039/c2fd20080edoi:10.1039/c2fd20080e

Accessed by



[UC-eLinks](#)[CrossRef](#)[Web of Science](#)[Google Scholar](#)

54. [↩](#)

1. A. C. Dumetz,
2. A. M. Chockla,
3. E. W. Kaler,
4. A. M. Lenhoff

, Protein phase behavior in aqueous solutions: Crystallization, liquid-liquid phase separation, gels, and aggregates. *Biophys. J.* **94**, 570-583 (2008).10.1529/biophysj.107.116152pmid:18160663 doi:10.1529/biophysj.107.116152

Accessed by



[UC-eLinks](#)[CrossRef](#)[PubMed](#)[Web of Science](#)[Google Scholar](#)

55. [↩](#)

1. D. Gebauer,
2. A. Völkel,

3. H. Cölfen
, Stable prenucleation calcium carbonate clusters. *Science* **322**, 1819–1822 (2008). 19095936pmid:19095936

Access provided by



[UC-eLinks](#)[Abstract](#)/[FREE Full Text](#)[Google Scholar](#)

56. [↵](#)

1. A. E. S. Van Driessche,
2. L. G. Benning,
3. J. D. Rodriguez-Blanco,
4. M. Ossorio,
5. P. Bots,
6. J. M. García-Ruiz

, The role and implications of bassanite as a stable precursor phase to gypsum precipitation. *Science* **336**, 69–72 (2012). 10.1126/science.1215648pmid:22491851 doi:10.1126/science.1215648

Access provided by



[UC-eLinks](#)[Abstract](#)/[FREE Full Text](#)[Google Scholar](#)

57. [↵](#)

1. J. Baumgartner,
2. A. Dey,
3. P. H. H. Bomans,
4. C. Le Coadou,
5. P. Fratzl,
6. N. A. Sommerdijk,
7. D. Faivre

, Nucleation and growth of magnetite from solution. *Nat. Mater.* **12**, 310–314 (2013).10.1038/nmat3558pmid:23377292 doi:10.1038/nmat3558

Access provided by



[UC-eLinks](#)[CrossRef](#)[PubMed](#)[Google Scholar](#)

58. [↵](#)

1. A. Navrotsky

, Energetic clues to pathways to biomineralization: Precursors, clusters, and nanoparticles. *Proc. Natl. Acad. Sci. U.S.A.* **101**, 12096–12101 (2004). 10.1073/pnas.0404778101pmid:15297621doi:10.1073/pnas.0404778101

Access provided by

Library

[UC-eLinks](#)[Abstract/FREE Full Text](#)[Google Scholar](#)

59. [↩](#)

1. A. Navrotsky

, Nanoscale effects on thermodynamics and phase equilibria in oxide systems. *ChemPhysChem* **12**, 2207–2215 (2011). 10.1002/cphc.201100129pmid:21744459doi:10.1002/cphc.201100129

Access provided by

Library

[UC-eLinks](#)[CrossRef](#)[PubMed](#)[Web of Science](#)[Google Scholar](#)

60. [↩](#)

1. D. S. Li,

2. F. Soberanis,

3. J. Fu,

4. W. T. Hou,

5. J. Z. Wu,

6. D. Kisailus

, Growth mechanism of highly branched titanium dioxide nanowires via oriented attachment. *Cryst. Growth Des.* **13**, 422–428 (2013). 10.1021/cg301388e doi:10.1021/cg301388e

Access provided by

Library

[UC-eLinks](#)[CrossRef](#)[Google Scholar](#)

61. [↩](#)

1. M. Raju,

2. A. C. T. van Duin,

3. K. A. Fichtorn

, Mechanisms of oriented attachment of TiO₂ nanocrystals in vacuum and humid environments: Reactive molecular dynamics. *Nano Lett.* **14**, 1836–1842 (2014). 10.1021/nl404533kpmid:24601782 doi:10.1021/nl404533k

Access provided by

Library

[UC-eLinks](#)[CrossRef](#)[PubMed](#)[Google Scholar](#)

62. [↵](#)

1. V. M. Yuwono,
2. N. D. Burrows,
3. J. A. Soltis,
4. R. L. Penn

, Oriented aggregation: Formation and transformation of mesocrystal intermediates revealed. *J. Am. Chem. Soc.* **132**, 2163–2165 (2010).10.1021/ja909769apmid:20112897 doi:10.1021/ja909769

a

ACCESS FULL BY

Library

[UC-eLinks](#)[CrossRef](#)[PubMed](#)[Web of Science](#)[Google Scholar](#)

63. [↵](#)

1. A. A. Gribb,
2. J. F. Banfield

, Particle size effects on transformation kinetics and phase stability in nanocrystalline TiO₂. *Am. Mineral.* **82**, 717–728 (1997).

ACCESS FULL BY

Library

[UC-eLinks](#)[Abstract](#)[Google Scholar](#)

64. [↵](#)

1. Y. Politi,
2. R. A. Metzler,
3. M. Abrecht,
4. B. Gilbert,
5. F. H. Wilt,
6. I. Sagi,
7. L. Addadi,
8. S. Weiner,
9. P. U. P. A. Gilbert

, Transformation mechanism of amorphous calcium carbonate into calcite in the sea urchin larval spicule. *Proc. Natl. Acad. Sci. U.S.A.* **105**, 17362–17366 (2008). 10.1073/pnas.0806604105pmid:18987314doi:10.1073/pnas.0806604105

ACCESS FULL BY

Library

[UC-eLinks](#)[Abstract](#)/[FREE Full Text](#)[Google Scholar](#)

65. [↶](#)

1. A. V. Radha,
2. T. Z. Forbes,
3. C. E. Killian,
4. P. U. P. A. Gilbert,
5. A. Navrotsky

, Transformation and crystallization energetics of synthetic and biogenic amorphous calcium carbonate. Proc. Natl. Acad. Sci. U.S.A. **107**,16438–16443 (2010). 10.1073/pnas.1009959107pmid:20810918 doi:10.1073/pnas.1009959107

UC eLinks ABSTRACT BY



[UC-eLinks](#)[Abstract/FREE Full Text](#)[Google Scholar](#)

66. [↶](#)

1. J. Rieger,
2. T. Frechen,
3. G. Cox,
4. W. Heckmann,
5. C. Schmidt,
6. J. Thieme

, Precursor structures in the crystallization/ precipitation processes of CaCO₃ and control of particle formation by polyelectrolytes. Faraday Discuss. **136**, 265–277, discussion 309–328 (2007). 10.1039/b701450cpmid:17955814doi:10.1039/b701450c

UC eLinks ABSTRACT BY



[UC-eLinks](#)[CrossRef](#)[PubMed](#)[Web of Science](#)[Google Scholar](#)

67.

1. S. Weiner,
2. I. Sagi,
3. L. Addadi

, Choosing the crystallization path less traveled. Science **309**, 1027–1028(2005). 10.1126/science.1114920pmid:16099970 doi:10.1126/science.1114920

UC eLinks ABSTRACT BY



[UC-eLinks](#)[Abstract/FREE Full Text](#)[Google Scholar](#)

68. [↵](#)

1. T. M. Davis,
2. T. O. Drews,
3. H. Ramanan,
4. C. He,
5. J. Dong,
6. H. Schnablegger,
7. M. A. Katsoulakis,
8. E. Kokkoli,
9. A. V. McCormick,
10. R. L. Penn,
11. M. Tsapatsis

, Mechanistic principles of nanoparticle evolution to zeolite crystals. *Nat. Mater.* **5**, 400–408 (2006). 10.1038/nmat1636 pmid:16617343 doi:10.1038/nmat1636

Accessed by

Library

[UC-eLinks](#)[CrossRef](#)[PubMed](#)[Google Scholar](#)

69. [↵](#)

1. E. M. Pouget,
2. P. H. H. Bomans,
3. A. Dey,
4. P. M. Frederik,
5. G. de With,
6. N. A. Sommerdijk

, The development of morphology and structure in hexagonal vaterite. *J. Am. Chem. Soc.* **132**, 11560–11565 (2010). 10.1021/ja102439r pmid:20669942 doi:10.1021/ja102439r

Accessed by

Library

[UC-eLinks](#)[CrossRef](#)[PubMed](#)[Web of Science](#)[Google Scholar](#)

70. [↵](#)

1. J. Ihli,
2. W. C. Wong,

3. E. H. Noel,
4. Y. Y. Kim,
5. A. N. Kulak,
6. H. K. Christenson,
7. M. J. Duer,
8. F. C. Meldrum

, Dehydration and crystallization of amorphous calcium carbonate in solution and in air. *Nat. Commun.* **5**,3169 (2014). 10.1038/ncomms4169pmid:24469266 doi:10.1038/ncomms4169

ACCESS BY



[UC-eLinks](#)[CrossRef](#)[PubMed](#)[Google Scholar](#)

71. [↵](#)

1. C. J. Stephens,
2. S. F. Ladden,
3. F. C. Meldrum,
4. H. K. Christenson

, Amorphous calcium carbonate is stabilized in confinement. *Adv. Funct. Mater.* **20**, 2108-2115 (2010).10.1002/adfm.201000248doi:10.1002/adfm.201000248

ACCESS BY



[UC-eLinks](#)[CrossRef](#)[Google Scholar](#)

72. [↵](#)

1. C. C. Tester,
2. R. E. Brock,
3. C. H. Wu,
4. M. R. Krejci,
5. S. Weigand,
6. D. Joester

, In vitro synthesis and stabilization of amorphous calcium carbonate (ACC) nanoparticles within liposomes. *CrystEngComm* **13**, 3975-3978(2011). 10.1039/c1ce05153adoi:10.1039/c1ce05153a

ACCESS BY



[UC-eLinks](#)[CrossRef](#)[Google Scholar](#)

73. [↩](#)

1. Q. Hu,
2. M. H. Nielsen,
3. C. L. Freeman,
4. L. M. Hamm,
5. J. Tao,
6. J. R. I. Lee,
7. T. Y. J. Han,
8. U. Becker,
9. J. H. Harding,
10. P. M. Dove,
11. J. J. De Yoreo

, The thermodynamics of calcite nucleation at organic interfaces: Classical vs. non-classical pathways. *Faraday Discuss.* **159**, 509–523 (2012).[10.1039/c2fd20124k](https://doi.org/10.1039/c2fd20124k)[doi:10.1039/c2fd20124k](https://doi.org/10.1039/c2fd20124k)

ACCESS FULLY BY

Library

[UC-eLinks](#)[CrossRef](#)[Web of Science](#)[Google Scholar](#)

74. [↩](#)

1. H. Zhang,
2. B. Gilbert,
3. F. Huang,
4. J. F. Banfield

, Water-driven structure transformation in nanoparticles at room temperature. *Nature* **424**, 1025–1029 (2003). [10.1038/nature01845](https://doi.org/10.1038/nature01845)
[id:1294496](https://doi.org/10.1038/nature01845)[doi:10.1038/nature01845](https://doi.org/10.1038/nature01845)

ACCESS FULLY BY

Library

[UC-eLinks](#)[CrossRef](#)[PubMed](#)[Google Scholar](#)

75. [↩](#)

1. L. Addadi,
2. S. Raz,
3. S. Weiner

, Taking advantage of disorder: Amorphous calcium carbonate and its roles in biomineralization. *Adv. Mater.* **15**, 959–970 (2003).[10.1002/adma.200300381](https://doi.org/10.1002/adma.200300381)[doi:10.1002/adma.200300381](https://doi.org/10.1002/adma.200300381)

76. [↵](#)

1. L. Yang,
2. C. E. Killian,
3. M. Kunz,
4. N. Tamura,
5. P. U. P. A. Gilbert

, Biomineral nanoparticles are space-filling. *Nanoscale* **3**, 603–609 (2011). 10.1039/C0NR00697Apmid:21082124 doi:10.1039/C0NR00697A

77. [↵](#)

1. C. C. Tester,
2. C. H. Wu,
3. M. R. Krejci,
4. L. Mueller,
5. A. Park,
6. B. Lai,
7. S. Chen,
8. C. J. Sun,
9. M. Balasubramanian,
10. D. Joester

, Time-resolved evolution of short- and long-range order during the transformation of amorphous calcium carbonate to calcite in the sea urchin embryo. *Adv. Funct. Mater.* **23**, 4185–4194 (2013). 10.1002/adfm.201203400doi:10.1002/adfm.201203400

78. [↵](#)

1. J. L. Zryd,
2. W. R. Burghardt

, Phase-separation, crystallization, and structure formation in immiscible polymer-solutions. J. Appl. Polym. Sci. **57**, 1525-1537 (1995).10.1002/app.1995.070571212doi:10.1002/app.1995.070571212

ACCESS FULLY BY
 [UC-eLinks](#)[CrossRef](#)[Google Scholar](#)

79. [↵](#)

1. W. L. Marshall,
2. C. E. Hall,
3. R. E. Mesmer

, The system dipotassium hydrogen phosphate-water at high temperatures (100–400°C): Liquid-liquid immiscibility and concentrated-solutions. J. Inorg. Nucl. Chem. **43**,449–455 (1981). 10.1016/0022-1902(81)80482-4doi:10.1016/0022-1902(81)80482-4

ACCESS FULLY BY
 [UC-eLinks](#)[CrossRef](#)[Google Scholar](#)

80. [↵](#)

1. H. Z. Zhang,
2. B. Chen,
3. Y. Ren,
4. G. A. Waychunas,
5. J. F. Banfield

, Response of nanoparticle structure to different types of surface environments: Wide-angle x-ray scattering and molecular dynamics simulations.Phys. Rev. B **81**, 125444 (2010). 10.1103/PhysRevB.81.125444doi:10.1103/PhysRevB.81.125444

4
ACCESS FULLY BY
 [UC-eLinks](#)[CrossRef](#)[Google Scholar](#)

81. [↵](#)

1. F. Huang,
2. B. Gilbert,
3. H. Zhang,
4. J. F. Banfield

, Reversible, surface-controlled structure transformation in nanoparticles induced by an aggregation state. Phys. Rev. Lett. **92**, 155501 (2004).10.1103/PhysRevLett.92.155501pmid:15169293 doi:10.1103/PhysRevLett.92.155501

Accessed by



[UC-eLinks](#)[CrossRef](#)[PubMed](#)[Google Scholar](#)

82. [↵](#)

1. F. M. Michel,
2. V. Barrón,
3. J. Torrent,
4. M. P. Morales,
5. C. J. Serna,
6. J. F. Boily,
7. Q. Liu,
8. A. Ambrosini,
9. A. C. Cismasu,
10. G. E. Brown Jr.

, Ordered ferrimagnetic form of ferrihydrite reveals links among structure, composition, and magnetism. Proc. Natl. Acad. Sci. U.S.A. **107**, 2787–2792 (2010).10.1073/pnas.0910170107pmid:20133643 doi:10.1073/pnas.0910170107

Accessed by



[UC-eLinks](#)[Abstract/FREE Full Text](#)[Google Scholar](#)

83. [↵](#)

1. T. Gibaud,
2. P. Schurtenberger

, A closer look at arrested spinodal decomposition in protein solutions. J. Phys. Condens. Matter **21**, 322201 (2009). 10.1088/0953-8984/21/32/322201pmid:21693959doi:10.1088/0953-8984/21/32/322201

Accessed by



[UC-eLinks](#)[CrossRef](#)[PubMed](#)[Google Scholar](#)

84. [↵](#)

A. A. Chernov, E. I. Givargizov, *Modern Crystallography III: Crystal Growth*. Springer Series in Solid-State Sciences (Springer, Berlin, 1984), vol. 36.

[Google Scholar](#)

85. [↵](#)

1. B. Derjaguin,
2. L. Landau

, Theory of stability of highly charged liophobic sols and adhesion of highly charged particles in solutions of electrolytes. Zhurnal Eksperimentalnoi Teor. Fiz. **15**, 663–682 (1945).

ACCESSIBLE BY

BERKELEY
Library
UNIVERSITY OF CALIFORNIA

[UC-eLinks](#)[Google Scholar](#)

86. [↵](#)

E. J. W. Verwey, J. T. G. Overbeek, K. van Nes, *Theory of the Stability of Lyophobic Colloids: The Interaction of Sol Particles Having an Electric Double Layer* (Elsevier, New York, 1948).

[Google Scholar](#)

87. [↵](#)

1. H. Zhang,
2. J. J. De Yoreo,
3. J. F. Banfield

, A unified description of attachment-based crystal growth. ACS Nano **8**, 6526–6530 (2014). 10.1021/nn503145wpmid:25000275 doi:10.1021/nn503145w

ACCESSIBLE BY

BERKELEY
Library
UNIVERSITY OF CALIFORNIA

[UC-eLinks](#)[CrossRef](#)[PubMed](#)[Google Scholar](#)

88. [↵](#)

1. H. Z. Zhang,
2. J. F. Banfield

, Energy calculations predict nanoparticle attachment orientations and asymmetric crystal formation. J. Phys. Chem. Lett. **3**, 2882–2886 (2012).10.1021/jz301161jdoi:10.1021/jz301161j

ACCESSIBLE BY

BERKELEY
Library
UNIVERSITY OF CALIFORNIA

[UC-eLinks](#)[CrossRef](#)[Google Scholar](#)

89. [↵](#)

1. G. V. Gibbs,
2. T. D. Crawford,
3. A. F. Wallace,
4. D. F. Cox,
5. R. M. Parrish,
6. E. G. Hohenstein,
7. C. D. Sherrill

, Role of long-range intermolecular forces in the formation of inorganic nanoparticle clusters. *J. Phys. Chem. A* **115**,12933–12940 (2011). 10.1021/jp204044kpmid:21939256 doi:10.1021/jp204044k

ACCESSible BY
 [UC-eLinks](#)[CrossRef](#)[PubMed](#)[Google Scholar](#)

90. [↵](#)

J. J. De Yoreo, P. G. Vekilov, in *Biomineralization*, P. M. Dove, J. J. DeYoreo, S. Weiner, Eds. (Mineralogical Society of America, Washington, DC, 2003), vol. 54, pp. 57–93.

[Google Scholar](#)

91. [↵](#)

1. L. O. Hedges,
2. S. Whitelam

, Patterning a surface so as to speed nucleation from solution. *Soft Matter* **8**,8624–8635 (2012). 10.1039/c2sm26038gdoi:10.1039/c2sm26038g

ACCESSible BY
 [UC-eLinks](#)[CrossRef](#)[Web of Science](#)[Google Scholar](#)

92. [↵](#)

1. A. J. Page,
2. R. P. Sear

, Heterogeneous nucleation in and out of pores. *Phys. Rev. Lett.* **97**, 065701 (2006).10.1103/PhysRevLett.97.065701pmid:17026175 doi:10.1103/PhysRevLett.97.065701

93. [↵](#)

1. Y. W. Wang,
2. H. K. Christenson,
3. F. C. Meldrum

, Confinement leads to control over calcium sulfate polymorph. Adv. Funct. Mater. **23**, 5615-5623 (2013).10.1002/adfm.201300861doi:10.1002/adfm.201300861

94. [↵](#)

1. C. C. Tester,
2. M. L. Whittaker,
3. D. Joester

, Controlling nucleation in giant liposomes. Chem. Commun. **50**,5619-5622 (2014). 10.1039/c4cc01457jpmid:24728476 doi:10.1039/c4cc01457j

95. [↵](#)

1. N. Vidavsky,
2. S. Addadi,
3. J. Mahamid,
4. E. Shimoni,
5. D. Ben-Ezra,
6. M. Shpigel,
7. S. Weiner,
8. L. Addadi

, Initial stages of calcium uptake and mineral deposition in sea urchin embryos. Proc. Natl. Acad. Sci. U.S.A. **111**,39-44 (2014). 10.1073/pnas.1312833110pmid:24344263 doi:10.1073/pnas.1312833110

96. [↵](#)

1. E. V. Shevchenko,
2. D. V. Talapin,
3. C. B. Murray,
4. S. O'Brien

, Structural characterization of self-assembled multifunctional binary nanoparticle superlattices. *J. Am. Chem. Soc.* **128**, 3620–3637 (2006). [10.1021/ja0564261](#) [pmid:16536535](#) [doi:10.1021/ja0564261](#)

97. [↵](#)

1. F. Nudelman,
2. K. Pieterse,
3. A. George,
4. P. H. H. Bomans,
5. H. Friedrich,
6. L. J. Brylka,
7. P. A. J. Hilbers,
8. G. de With,
9. N. A. Sommerdijk

, The role of collagen in bone apatite formation in the presence of hydroxyapatite nucleation inhibitors. *Nat. Mater.* **9**, 1004–1009 (2010). [10.1038/nmat2875](#) [pmid:20972429](#) [doi:10.1038/nmat2875](#)

98. [↵](#)

1. D. Gebauer,
2. H. Cölfen,
3. A. Verch,
4. M. Antonietti

, The multiple roles of additives in CaCO₃ crystallization: A quantitative case study. Adv. Mater. **21**, 435-439 (2009).10.1002/adma.200801614doi:10.1002/adma.200801614

Accessed by



[UC-eLinks](#)[CrossRef](#)[Web of Science](#)[Google Scholar](#)

99. [↩](#)

1. T. Kato

, Polymer/calcium carbonate layered thin-film composites. Adv. Mater. **12**, 1543-1546 (2000). 10.1002/1521-4095(200010)12:20<1543::AID-ADMA1543>3.0.CO;2-Pdoi:10.1002/1521-4095(200010)12:20<1543::AID-ADMA1543>3.0.CO;2-P

Accessed by



[UC-eLinks](#)[CrossRef](#)[Google Scholar](#)

100. [↩](#)

1. B. Cantaert,
2. Y. Y. Kim,
3. H. Ludwig,
4. F. Nudelman,
5. N. A. J. M. Sommerdijk,
6. F. C. Meldrum

, Think positive: Phase separation enables a positively charged additive to induce dramatic changes in calcium carbonate morphology. Adv. Funct. Mater. **22**, 907-915 (2012).10.1002/adfm.201102385doi:10.1002/adfm.201102385

Accessed by



[UC-eLinks](#)[CrossRef](#)[Google Scholar](#)

101. [↩](#)

1. J. J. M. Lenders,
2. C. L. Altan,
3. P. H. H. Bomans,
4. A. Arakaki,
5. S. Bucak,
6. G. de With,


7. N. A. J. M. Sommerdijk
, A bioinspired coprecipitation method for the controlled synthesis of magnetite nanoparticles. *Cryst. Growth Des.* **14**, 5561–5568 (2014). 10.1021/cg500816zdoi:10.1021/cg500816z

ACCESS FULL BY
 [UC-eLinksCrossRefGoogle Scholar](#)

102. [↩](#)

1. M. Suzuki,
2. K. Saruwatari,
3. T. Kogure,
4. Y. Yamamoto,
5. T. Nishimura,
6. T. Kato,
7. H. Nagasawa

, An acidic matrix protein, Pif, is a key macromolecule for nacre formation. *Science* **325**, 1388–1390 (2009).10.1126/science.1173793p mid:19679771 doi:10.1126/science.1173793

ACCESS FULL BY
 [UC-eLinksAbstract/FREE Full TextGoogle Scholar](#)

103.

1. I. M. Weiss,
2. S. Kaufmann,
3. K. Mann,
4. M. Fritz

, Purification and characterization of perlucin and perlustrin, two new proteins from the shell of the mollusc *Haliothis laevigata*. *Biochem. Biophys. Res. Commun.* **267**, 17–21(2000). 10.1006/bbrc.1999.1907pmid:10623567 doi:10.1006/bbrc.1999.1907

ACCESS FULL BY
 [UC-eLinksCrossRefPubMedWeb of ScienceGoogle Scholar](#)

104.

1. G. Fu,
2. S. Valiyaveetil,

3. B. Wopenka,

4. D. E. Morse

, CaCO₃ biomineralization: Acidic 8-kDa proteins isolated from aragonitic abalone shell nacre can specifically modify calcite crystal morphology. *Biomacromolecules* **6**, 1289–1298 (2005). 10.1021/bm049314vpmid:15877344 doi:10.1021/bm049314v



[UC-eLinks](#)[CrossRef](#)[PubMed](#)[Web of Science](#)[Google Scholar](#)

105. [↩](#)

1. R. A. Metzler,

2. J. S. Evans,

3. C. E. Killian,

4. D. Zhou,

5. T. H. Churchill,

6. N. P. Appathurai,

7. S. N. Coppersmith,

8. P. U. P. A. Gilbert

, Nacre protein fragment templates lamellar aragonite growth. *J. Am. Chem. Soc.* **132**, 6329–6334(2010). 10.1021/ja909735ypmid:20397648 doi:10.1021/ja909735y



[UC-eLinks](#)[CrossRef](#)[PubMed](#)[Google Scholar](#)

106. [↩](#)

1. R. F. Lobo,

2. S. I. Zones,

3. M. E. Davis

, Structure-direction in zeolite synthesis. *J. Incl. Phenom. Mol. Recogn. Chem.* **21**, 47–78 (1995).



[UC-eLinks](#)[Google Scholar](#)

107. [↩](#)

1. J. F. Banfield,

2. S. A. Welch,

3. H. Zhang,
4. T. T. Ebert,
5. R. L. Penn

, Aggregation-based crystal growth and microstructure development in natural iron oxyhydroxide biomineralization products. *Science* **289**, 751–754 (2000). 10.1126/science.289.5480.751
pmid:10926531 doi:10.1126/science.289.5480.751

Accessed by



[UC-eLinks](#)[Abstract](#)/[FREE Full Text](#)[Google Scholar](#)

108. [↩](#)

1. J. P. Grotzinger,
2. A. H. Knoll

, Stromatolites in Precambrian carbonates: Evolutionary mileposts or environmental dipsticks? *Annu. Rev. Earth Planet. Sci.* **27**, 313–358 (1999).10.1146/annurev.earth.27.1.313
pmid:11543060 doi:10.1146/annurev.earth.27.1.313

Accessed by



[UC-eLinks](#)[CrossRef](#)[PubMed](#)[Web of Science](#)[Google Scholar](#)

109. [↩](#)

1. M. Kuno

, An overview of solution-based semiconductor nanowires: Synthesis and optical studies. *Phys. Chem. Chem. Phys.* **10**, 620–639 (2008). 10.1039/B708296G
pmid:19791445 doi:10.1039/B708296G

Accessed by



[UC-eLinks](#)[CrossRef](#)[PubMed](#)[Google Scholar](#)

110. [↩](#)

1. D. B. Suyatin,
2. J. Sun,
3. A. Fuhrer,
4. D. Wallin,
5. L. E. Fröberg,
6. L. S. Karlsson,
7. I. Maximov,
8. L. R. Wallenberg,

9. L. Samuelson,

10. H. Q. Xu

, Electrical properties of self-assembled branched InAs nanowire junctions. *Nano Lett.* **8**, 1100–1104 (2008). 10.1021/nl073193ypmid:18355057 doi:10.1021/nl073193

y



[UC-eLinks](#)[CrossRef](#)[PubMed](#)[Web of Science](#)[Google Scholar](#)

111. [↩](#)

1. M. J. Bierman,

2. S. Jin

, Potential applications of hierarchical branching nanowires in solar energy conversion. *Energy Environ. Sci.* **2**, 1050–1059 (2009). 10.1039/b912095e doi:10.1039/b912095e



[UC-eLinks](#)[CrossRef](#)[Google Scholar](#)

112. [↩](#)

1. I. Herman,

2. J. Yeo,

3. S. Hong,

4. D. Lee,

5. K. H. Nam,

6. J. H. Choi,

7. W. H. Hong,

8. D. Lee,

9. C. P. Grigoropoulos,

10. S. H. Ko

, Hierarchical weeping willow nano-tree growth and effect of branching on dye-sensitized solar cell efficiency. *Nanotechnology* **23**, 194005 (2012). 10.1088/0957-4484/23/19/194005pmid:22538967doi:10.1088/0957-4484/23/19/194005



[UC-eLinks](#)[CrossRef](#)[PubMed](#)[Google Scholar](#)

113. [↩](#)

1. L. Zhou,
 2. P. O'Brien
- , Mesocrystals: A new class of solid materials. *Small* **4**, 1566–1574 (2008).10.1002/sml.200800520pmid:18844308 doi:10.1002/sml.200800520

ACCESSible BY



[UC-eLinks](#)[CrossRef](#)[PubMed](#)[Web of Science](#)[Google Scholar](#)

114. [↵](#)

1. S. Furukawa,
2. J. Reboul,
3. S. Diring,
4. K. Sumida,
5. S. Kitagawa

, Structuring of metal-organic frameworks at the mesoscopic/macroscopic scale. *Chem. Soc. Rev.* **43**, 5700–5734 (2014).10.1039/C4CS00106Kpmid:24811425 doi:10.1039/C4CS00106K

ACCESSible BY



[UC-eLinks](#)[CrossRef](#)[PubMed](#)[Google Scholar](#)

115. [↵](#)

1. M. E. Davis

, Ordered porous materials for emerging applications. *Nature* **417**, 813–821 (2002).10.1038/nature00785pmid:12075343 doi:10.1038/nature00785

ACCESSible BY



[UC-eLinks](#)[CrossRef](#)[PubMed](#)[Web of Science](#)[Google Scholar](#)

116. [↵](#)

1. R. L. Penn,
2. J. F. Banfield

, Morphology development and crystal growth in nanocrystalline aggregates under hydrothermal conditions: Insights from titania. *Geochim. Cosmochim. Acta* **63**, 1549–1557 (1999).10.1016/S0016-7037(99)00037-Xdoi:10.1016/S0016-7037(99)00037-X

ACCESSible BY



[UC-eLinks](#)[CrossRef](#)[Web of Science](#)[Google Scholar](#)

117. [↵](#)

1. S. Kumar,
2. Z. Wang,
3. R. L. Penn,
4. M. Tsapatsis

, A structural resolution cryo-TEM study of the early stages of MFI growth. *J. Am. Chem. Soc.* **130**, 17284-17286 (2008). 10.1021/ja8063167pmid:19049299doi:10.1021/ja8063167

ACCESSible BY



[UC-eLinks](#)[CrossRef](#)[PubMed](#)[Web of Science](#)[Google Scholar](#)

118. [↵](#)

1. Y. Oaki,
2. H. Imai

, The hierarchical architecture of nacre and its mimetic material. *Angew. Chem. Int. Ed.* **44**, 6571-6575 (2005). 10.1002/anie.200500338pmid:16163773 doi:10.1002/anie.200500338

ACCESSible BY



[UC-eLinks](#)[CrossRef](#)[PubMed](#)[Google Scholar](#)

119. [↵](#)

1. J. Mahamid,
2. B. Aichmayer,
3. E. Shimoni,
4. R. Ziblat,
5. C. Li,
6. S. Siegel,
7. O. Paris,
8. P. Fratzl,
9. S. Weiner,
10. L. Addadi

, Mapping amorphous calcium phosphate transformation into crystalline mineral from the cell to the bone in zebrafish fin rays. *Proc. Natl. Acad. Sci. U.S.A.* **107**, 6316-

6321 (2010).10.1073/pnas.0914218107pmid:20308589 doi:10.1073/pnas.0914218107

ACCESSible BY



[UC-eLinks](#)[Abstract/FREE Full Text](#)[Google Scholar](#)

120. [←](#)

1. V. K. Ivanov,
2. P. P. Fedorov,
3. A. Y. Baranchikov,
4. V. V. Osiko

, Oriented attachment of particles: 100 years of investigations of non-classical crystal growth. *Russ. Chem. Rev.* **83**, 1204–1222 (2014).10.1070/RCR4453doi:10.1070/RCR4453

ACCESSible BY



[UC-eLinks](#)[CrossRef](#)[Google Scholar](#)

121. **Acknowledgments:** This article evolved from presentations and discussions at the workshop “Crystallization by Particle Attachment” held in December 2013 in Berkeley, California, sponsored by the Council on Geosciences of the U.S. Department of Energy, Office of Science, Office of Basic Energy Sciences. The authors thank the members of the council for their encouragement and assistance in developing this workshop. We also thank L. Addadi and S. Weiner for valuable comments and advice. In addition, the authors acknowledge the agencies that provided funding for their individual research programs, without which this workshop and article would not have been possible.

[View Abstract](#)